Pyruvate:ferredoxin oxidoreductase and low abundant ferredoxins support aerobic photomixotrophic growth in cyanobacteria

Yingying Wang[a], Xi Chen[a], Katharina Spengler[a], Karoline Terberger[a], Marko Boehm[a,b], Jens Appel[a,b], Thomas Barske[c], Stefan Timm[c], Natalia Battchikova[d], Martin Hagemann[c], Kirstin Gutekunst[a,b]

[a]Department of Biology, Botanical Institute, Christian-Albrechts-University, D-24118 Kiel, Germany; [b]Department of Molecular Plant Physiology, Bioenergetics in Photoautotrophs, University of Kassel, D-34132 Kassel, Germany, [c]Plant Physiology Department, University of Rostock, D-18059 Rostock, Germany, [d]Department of Biochemistry, Molecular Plant Biology, University of Turku, FI-20014 Turku, Finnland

*Kirstin Gutekunst

Email: kirstin.gutekunst@uni-kassel.de

Competing Interest Statement: The authors declare no conflict of interest.

Keywords: cyanobacteria, ferredoxin, GOGAT, pyruvate dehydrogenase

Abstract

The decarboxylation of pyruvate is a central reaction in the carbon metabolism of all organisms. It is catalyzed by the pyruvate:ferredoxin oxidoreductase (PFOR) and the pyruvate dehydrogenase (PDH) complex. Whereas PFOR reduces ferredoxin, the PDH complex utilizes NAD^+. Anaerobes rely on PFOR, which was replaced during evolution by the PDH complex found in aerobes. Cyanobacteria possess both enzyme systems. Our data challenge the view that PFOR is exclusively utilized for fermentation. Instead, we show, that the cyanobacterial PFOR is stable in the presence of oxygen *in vitro* and is required for optimal photomixotrophic growth under aerobic and highly reducing conditions while the PDH complex is inactivated. We found that cells rely on a general shift from utilizing NAD(H)-dependent to ferredoxin-dependent enzymes under these conditions.

The utilization of ferredoxins instead of NAD(H) saves a greater share of the Gibbs free energy, instead of wasting it as heat. This obviously simultaneously decelerates metabolic reactions as they operate closer to their thermodynamic equilibrium. It is common thought that during evolution, ferredoxins were replaced by NAD(P)H due to their higher stability in an oxidizing atmosphere. However, utilization of NAD(P)H could also have been favored due to a higher competitiveness because of an accelerated metabolism.

Introduction

FeS clusters, pyruvate:ferredoxin oxidoreductase and ferredoxins

Life evolved under anaerobic conditions in an environment that was reducing and replete with iron and sulfur. Later on, hydrogen escape to space irreversibly oxidized Earth (1, 2). Prebiotic redox reactions that took place on the surfaces of FeS minerals, are at present mimicked by catalytic FeS clusters in a plethora of enzymes and redox carriers (3, 4). One example are ferredoxins, that are small, soluble proteins containing 4Fe4S, 3Fe4S or 2Fe2S clusters and shuttle electrons between redox reactions. They display a wide range of redox potentials between -240 mV to -680 mV and are involved in a variety of metabolic pathways (5). Ferredoxins are among the earliest proteins on Earth and are accordingly present in all three kingdoms of life (6). FeS enzymes are especially widespread in anaerobes (7).

The advent of oxygenic photosynthesis necessitated adaptations, as especially 4Fe4S clusters are oxidized and degraded to 3Fe4S in the presence of oxygen resulting in inactivated enzymes (7-9). In aerobes, FeS enzymes are commonly replaced by FeS cluster free isoenzymes or alternative metabolic strategies (8). One well known example is the replacement of the FeS cluster containing pyruvate:ferredoxin oxidoreductase (PFOR), which catalyzes the decarboxylation of pyruvate during fermentation in anaerobes, by the pyruvate dehydrogenase (PDH) complex for respiration in aerobes (7, 10). Both enzymes catalyze the same reaction, however, PFOR uses ferredoxin as redox partner and the PDH complex reduces NAD^+. PFORs are old enzymes from an evolutionary point of view. They are widespread in autotrophic and heterotrophic bacteria, in archaea, amitochondriate eukaryotic protists, hydrogenosomes as well as in cyanobacteria and algae (7). Depending on organism, metabolism and conditions, PFOR can be involved in the oxidation of pyruvate for heterotrophy or alternatively catalyze the reverse reaction by fixing CO_2 and forming pyruvate from acetyl CoA for an autotrophic lifestyle (11-13). The enzyme might have played a central role for the evolution of both autotrophic and heterotrophic processes from the very beginning (14). PFOR indeed participates as CO_2 fixing enzyme in four out of seven currently known and most ancient autotrophic pathways (reverse tricarboxylic acid (rTCA) cycle, reversed oxidative tricarboxylic acid (roTCA) cycle, reductive acetyl-CoA pathway, and dicarboxylate/hydroxybutyrate (DC/HB) cycle) (12, 15). PFORs contain one to three 4Fe4S clusters and in general get inactivated readily by oxygen upon purification. So far, there are only three reported exceptions to this rule: the PFORs of *Halobacterium halobium*, *Desulvovibrio africanus* and *Sulfolobus acidocaldarius* (11, 16-19). Even though all three enzymes are stable upon purification in the presence of oxygen, anaerobic conditions are required for *in vitro* maintenance of enzyme activities with the PFORs of *Desulvovibrio africanus* and *Sulfolobus acidocaldarius.* The enzyme of *Halobacterium halobium* is the only PFOR reported so far, which is active under aerobic conditions *in vitro* (19, 20). *In vivo* studies on these PFORs under aerobic conditions are missing. Recently it was shown in *E. coli*, that PFOR plays an important role in aerobic cultures of a mutant in which glucose-6P dehydrogenase (ZWF) was down-regulated (21). PFOR is probably involved in redox control during stationary phase in this mutant (21). This finding is highly surprising, as PFOR activity in *E. coli* crude extracts is only detectable under anaerobic conditions *in vitro* (22). There are several reports on the aerobic expression of enzymes that are assigned to anaerobic metabolism in prokaryotes and eukaryotes and therefore challenge the simplistic distinction between aerobic versus anaerobic enzymes (10, 23, 24). Their physiological significance and regulation are only partly understood.

Ferredoxins that contain 4Fe4S clusters are likewise vulnerable to oxidative degradation. In the evolution from anoxygenic to oxygenic photosynthesis, the soluble 4Fe4S ferredoxin, which

transfers electrons from FeS-type photosystems PSI to other enzymes in anoxygenic photosynthesis was replaced by an oxygen-tolerant 2Fe2S ferredoxin (9). In addition, NAD(P)H has gained importance as alternative, oxygen-insensitive reducing agent in aerobes and thereby complemented or replaced oxygen sensitive ferredoxins, that are useful for anaerobes (10).

The pyruvate dehydrogenase complex

The PDH complex, which utilizes NAD^+ is composed of the three subunits: pyruvate dehydrogenase (E1), dihydrolipoyl transacetylase (E2) and dihydrolipoyl dehydrogenase (E3). It catalyzes the irreversible decarboxylation of pyruvate. The PDH complex is active under oxic conditions but gets inactivated under anaerobic conditions in both prokaryotes and eukaryotes, albeit via distinct mechanisms. In the absence of oxygen $NADH/NAD^+$ ratios rise as respiration no longer oxidizes the NADH coming from the PDH complex and the subsequent reactions of the TCA cycle. In prokaryotes, as e.g. *E. coli*, NADH interacts with the dihydrolipoyl dehydrogenase (E3) subunit and thereby inhibits the PDH complex (25, 26). In eukaryotes, the PDH complex gets inactivated at high $NADH/NAD^+$ ratios via phosphorylation of highly conserved serine residues in the pyruvate dehydrogenase (E1) subunit (27).

Synechocystis sp. PCC 6803 is a cyanobacterium that performs oxygenic photosynthesis and lives photoautotrophically by fixing CO_2 via the Calvin-Benson-Bassham (CBB) cycle. In the presence of external carbohydrates these are metabolized additionally, resulting in a photomixotrophic lifestyle. In darkness *Synechocystis* switches to a heterotrophic or under anaerobic conditions to a fermentative lifestyle. As in many cyanobacteria, pyruvate can be either decarboxylated via PFOR or alternatively via the PDH complex in *Synechocystis.* PFOR is assumed to be involved in fermentation under anoxic conditions and the PDH complex in aerobic respiration. The observation that *pfor* is transcribed under photoautotrophic conditions in the presence of oxygen in the cyanobacteria *Synechococcus* sp. PCC 7942 and *Synechocystis* was therefore surprising but is well in line with the observation that other enzymes assigned to anaerobic metabolism in eukaryotes are expressed in the presence of oxygen as well (10, 23). *Synechoystis* possesses a network of up to 11 ferredoxins containing 2Fe2S, 3Fe4S and 4Fe4S clusters (28, 29). The 2Fe2S ferredoxin 1 (Ssl0020) is essential and by far the most abundant ferredoxin in *Synechocystis* and is the principal acceptor of photosynthetic electrons at PSI (30). Structures, redox potentials and distinct functions have been resolved for some of the alternative low abundant ferredoxins, however, the metabolic significance of the complete network is still far from being understood (28, 29, 31-34).

In this study we show that PFOR and low abundant ferredoxins are required for optimal photomixotrophic growth under oxic conditions. In line with this we found that the cyanobacterial PFOR is stable in the presence of oxygen *in vitro*. PFOR and ferredoxins can functionally replace the NAD^+ dependent PDH complex, which we found is inactivated at high $NADH/NAD^+$ ratios. Likewise, the ferredoxin dependent F-GOGAT (glutamine oxoglutarate aminotransferase) is essential for photomixotrophic growth as well and cannot be functionally replaced by the NADH dependent N-GOGAT. The cells obviously switch in their utilization of isoenzymes and redox pools. However, the key factor for this switch is not oxygen but are the highly reducing conditions within the cells. Our data suggest that the pool of ferredoxins in *Synechocystis* functions as an overflow basin to shuttle electrons, when the $NADH/NAD^+$ pool is highly reduced.

Results

The roles of PDH complex and PFOR were studied in *Synechocystis* under different growth conditions. PDH could not be deleted from the genome indicating that this enzyme complex is essential, whereas *pfor* was knocked out in a previous study (31). In line with this, we found that all fully sequenced diazotrophic and non-diazotrophic cyanobacteria with PSII contain genes coding for a PDH complex and that 56 % of these cyanobacteria possess a PFOR as well. If we subtract from this group all diazotrophic cyanobacteria that contain a nitrogenase and might therefore utilize PFOR in the process of nitrogen fixation, 130 non-diazotrophic cyanobacteria remain. Within the group of non-diazotrophic cyanobacteria 42% possess a PFOR in addition to the PDH complex (Figure 1 – figure supplement figure 1). This clearly shows that the property of holding both a PDH complex and a PFOR in cyanobacteria that live predominantly under oxic conditions is truly widespread. The analysis furthermore confirms our observation, that the PDH complex is preferred over the utilization of PFOR in cyanobacteria.We unexpectedly found that the *Synechocystis* Δ*pfor* deletion mutant was impaired in its photomixotrophic growth under oxic conditions in continuous light. Growth impairment was typically visible starting around day three to six of the growth experiment (Figures 1A and 3A). In addition, maintenance in the stationary growth phase was affected in Δ*pfor*. Under photoautotrophic conditions Δ*pfor* grew similar to the WT (Figure 1A). The oxygen concentration in the photomixotrophic cultures was close to saturation around 250 µMol O_2 throughout the growth experiment (Figure 1 – figure supplement figure 2). Studies on the transcription of *pfor* and the alpha subunit of the pyruvate dehydrogenase (E1) of *pdhA* revealed that both genes are transcribed under photomixo- and photoautotrophic conditions (Figure 1 – figure supplement figure 3). These observations raised two questions: Why is the PDH complex, which catalyzes the same reaction as PFOR, not able to compensate for the loss of PFOR? And how can PFOR, which is assumed to be oxygen-sensitive, be of physiological relevance in the presence of oxygen?

The most obvious assumption is that the PDH complex might get inactivated under photomixotrophic conditions. As the PDH complex gets inactivated at high NADH/NAD^+ ratios in prokaryotes and eukaryotes (25-27), we wondered if NADH/NAD^+ ratios might be increased under photomixotrophic conditions. Corresponding measurements confirmed this assumption. Whereas NADH/NAD^+ ratios were stable under photoautotrophic conditions in WT and Δ*pfor* they raised three to fourfold in the first five days of photomixotrophic growth, exactly in that period in which the growth impairment of Δ*pfor* in the presence of glucose was most apparent (Figure 1B).

In addition, *in vivo* NAD(P)H fluorescence measurements and estimates for the reduction level of ferredoxin using a Dual-KLAS/NIR were performed, which show that in addition to the NADH/NAD^+ ratio, also the NAD(P)H and ferredoxin pools are more reduced under photomixotrophic conditions in comparison to photoautotrophic conditions (Figure 1 – figure supplement figure 4).

For prokaryotes it was shown that the PDH complex is inhibited by a distinct mechanism directly by NADH which binds to the dihydrolipoyl dehydrogenase (E3) subunit of the PDH complex (25, 26). Therefore, the recombinant dihydrolipoyl dehydrogenase of *Synechocystis* (SynLPD) was tested in an *in vitro* assay with different NADH concentrations. The enzyme indeed loses activity at higher NADH/NAD^+ ratios, whereas NADPH has no effect (Figure 2A). The SynLPD activity was completely inhibited by NADH with an estimated Ki of 38.3 µM (Figure 2A). Hence, the enzyme activity dropped to approximately 50% at a NADH/NAD^+ ratio of 0.1 (e.g. at 0.2 mM NADH in the presence of 2 mM NAD^+). Please note, that much higher NADH/NAD^+ ratios (> 0.4) were

measured in photomixotrophic cells of *Synechocystis* (see Figure 1B). This points to an efficient inhibition of PDH activity via the highly decreased function of the E3 subunit (SynLPD). NADH/NAD^+ ratios above 0.1 could not be tested in the enzyme assays due to the high background absorption of the added NADH, which prevented SynLPD activity detections.

Taken together these measurements convincingly show that the PDH complex is most likely inhibited under photomixotrophic conditions at high NADH/NAD^+ ratios, which provides evidence that pyruvate oxidation must be performed instead via PFOR and gives an explanation for the importance of PFOR under these conditions.

As the cyanobacterial PFOR is regarded as an oxygen sensitive enzyme that exclusively supports fermentation under anaerobic conditions, we overexpressed the enzyme and purified it in the presence of oxygen in order to check for its stability under aerobic conditions (Figure 2 – figure supplement 1, Figure 2 – figure supplement 2, Figure 2 – figure supplement 3). Enzymatic tests revealed that PFOR from *Synechocystis* was indeed stable under aerobic conditions *in vitro*, which means that the enzyme was not degraded and kept its activity but required anoxic conditions for the decarboxylation of pyruvate (Figure 2B) as reported for the oxygen stable PFORs of *Desulvovibrio africanus* and *Sulfolobus acidocaldarius (11, 16).*

In contrast to the PDH complex, PFOR transfers electrons from pyruvate to oxidized ferredoxin. In order to investigate if any of the low abundant ferredoxins (Fx) might be of importance for photomixotrophic growth, respective deletion mutants were generated (Supplementary File 1a and 1b, Figure 3 – figure supplement 1) and tested for their ability to grow under photoautotrophic and photomixotrophic conditions. To this end *fx3* (*slr1828*), *fx4* (*slr0150*), *fx6* (*ssl2559*), *fx7* (*sll0662*) and *fx9* (*slr2059*) could be completely deleted from the genome, whereas the deleted alleles of *fx2* (*sll1382*) and *fx5* (*slr0148*) failed to segregate, keeping some wild type copies. Furthermore, we did not succeed to delete *fx8* (*ssr3184*). Flavodoxin (*isiB; sll0284*), which replaces ferredoxins functionally under Fe-limitation was deleted as well. In addition, the double mutants Δ*fx7*Δ*fx9* and Δ*fx9*Δ*isiB* as well as the triple mutant Δ*fx7*Δ*fx8*Δ*fx9* were generated. Photoautotrophic growth of all these ferredoxin deletion mutants was similar to the WT (Figure 3 – figure supplement 2). However, under photomixotrophic conditions deletion of either *fx3*, *fx9* or flavodoxin (*isiB*) resulted in a growth behavior that was similar to Δ*pfor* (Figure 3A).

These results indicate that there might be a general shift to utilize the ferredoxin pool as soon as the NADH/NAD^+ pool is over-reduced. Beside the PFOR/PDH complex couple, GOGAT (glutamine oxoglutarate aminotransferase) as well is present in form of two isoenzymes in *Synechocystis* that either utilizes reduced ferredoxin (F-GOGAT; *sll1499*) or NADH (N-GOGAT; *sll1502*). In line with our assumption that ferredoxin utilization is preferred in over-reduced cells after glucose addition, we hypothesized that F-GOGAT might be required for optimal photomixotrophic growth. Respective deletion mutants were generated (Supplementary File 1a and 1b, Figure 3 – figure supplement 1) and revealed that neither Δ*f-gogat* nor Δ*n-gogat* were impaired in their growth under photoautotrophic conditions, whereas Δ*f-gogat* displayed a strong growth impairment under photomixotrophic conditions in contrast to Δ*n-gogat* and the WT (Figure 3B). These data indicate that cells indeed rely on a general switch from utilizing NAD(H) to utilizing ferredoxins for optimal photomixotrophic growth. It was recently shown that photosynthetic complex I (NDH1) exclusively accepts electrons from reduced ferredoxin instead of NAD(P)H (35). Under photomixotrophic conditions photosynthesis operates in parallel to carbon oxidation. In addition to water oxidation at photosystem II (PSII), electrons from glucose

oxidation can as well enter the respiratory/photosynthetic electron transport chain and eventually arrive at photosystem I (PSI). Photosynthesis based on PSI thus uses electrons from glucose oxidation that enter the respiratory/photosynthetic electron transport chain and are excited at PSI.

Three entry points exist that can feed electrons from glucose oxidation into the plastoquinone (PQ) pool in the thylakoid membrane: the succinate dehydrogenase (SDH), which accepts electrons from the conversion of succinate to fumarate; NDH-2, which accepts electrons from NADH and photosynthetic complex I (NDH-1), which accepts electrons from reduced ferredoxin (see Figure 4B). Based on the observed shift from utilizing ferredoxin instead of NAD(P)H, we thus wondered if photosynthetic complex I (NDH-1) might be required for photosynthesis (involving only PSI) under photomixotrophic conditions as an entry point for electrons coming from glucose oxidation. Cells were incubated with DCMU that blocks the electron transfer from PSII to the PQ-pool. Thereby, electron transfer from glycogen or glucose oxidation to PSI could be measured based on a recently developed protocol (36). According to this protocol electrons were counted that flow through PSI via $DIRK_{PSI}$ measurements by the KLAS/NIR instrument. The electron transport at PSI was then measured in the absence and in the presence of glucose. In addition to the WT, several mutants were analyzed with deletions in entry points as well as glucose metabolizing enzymes. The mutant with a deleted photosynthetic complex I (Δ*ndhD1*Δ*ndhD2*) should no longer be able to feed electrons from reduced ferredoxin into the respiratory/photosynthetic electron transport chain, while the hexokinase mutant (Δ*hk*) should no longer be able to metabolize external glucose. The glycogen phosphorylase mutant (Δ*glgP1*Δ*glgP2*) is unable to break down its internal glycogen reservoir (36-38). As expected and in parts shown recently (36), addition of glucose resulted in higher donations of electrons to PSI in the WT and Δ*glgP1*Δ*glgP2*, whereas neither Δ*ndhD1*Δ*ndhD2* nor Δ*hk* were able to provide electrons from glucose oxidation to PSI (Figure 3C). Photosynthesis using glucose oxidation and PSI thus relies on the ferredoxin dependent photosynthetic complex I. In line with this, it was shown earlier that Δ*ndhD1*Δ*ndhD2* is not able to grow in the presence of glucose and DCMU under photoheterotrophic conditions (39).

Discussion

Under photomixotrophic conditions, photosynthesis and glucose oxidation operate in parallel. The cells are thus flooded with electrons from water oxidation at PSII and electrons from glucose oxidation (Figure 4). This causes highly reducing conditions in the cells as visible in reduced NAD(P)H and ferredoxin pools (Figure 1B and Figure 1 – figure supplement 1). Our data indicate that the PDH complex gets inhibited at high NADH levels under these conditions and is subsequently most likely functionally replaced by PFOR (Figures 1 and 2). Furthermore, the cells seem to rely on a general shift from utilizing NAD(H)-dependent to ferredoxin-dependent enzymes under these conditions. In line with this, low abundant ferredoxins, whose functions are still only partly understood in detail, and ferredoxin-dependent F-GOGAT are required for optimal photomixotrophic performance (Figure 3). Photosynthetic complex I (NDHI) which accepts electrons from reduced ferredoxin (35), is furthermore required to feed electrons from glucose oxidation into the photosynthetic electron chain and to thereby enhance electron flow at PSI (Figures 3 and 4).

PFORs are with a few reported exceptions highly oxygen sensitive enzymes that work under strictly anaerobic conditions (16, 18, 19). We found that PFOR of *Synechocystis* is stable in the presence of oxygen, however, *in vitro* we could only measure the decarboxylation of pyruvate in

the absence of oxygen (Figure 2). However, our data strongly indicate that this enzyme is active *in vivo* under aerobic and highly reducing conditions.

Similar results were recently reported for *E. coli*. *E.coli* possesses three enzyme systems to convert pyruvate to acetyl CoA: the PDH complex, PFOR and pyruvate formate-lyase (PFL) (40). The PDH complex and PFL are the principle enzyme systems to convert pyruvate to acetylCoA in *E.coli*, whereas PFOR is expressed at very low levels (40). Transcription of PFOR was shown to be enhanced under oxidative stress (22). *E. coli* decarboxylates pyruvate via the PDH complex in the presence of oxygen. Under anaerobic conditions NADH levels rise and inhibit the PDH complex. PFL gets activated and the cells switch to fermentation. PFL activation requires reduced flavodoxin which is provided by PFOR (40). The regulation at the pyruvate node in *E. coli* is thus mainly regulated via the availability of oxygen and its concomitant requirement for redox control and ATP (41). By down-regulation of glucose-6P dehydrogenase (ZWF), less NADPH was produced in *E.coli*, which activated the expression of PFOR and ferredoxin reductase (FPR) (21). PFOR and FPR were shown to contribute to stationary phase metabolism in aerobic cultures in this mutant probably by converting reduced ferredoxin to NADPH (21). PFOR is thus obviously involved in redox control in these mutants in the presence of oxygen. This finding was highly unexpected, as PFOR activity in crude extracts from aerobically grown E.coli cells is only detectable in the absence of oxygen *in vitro* (22).There are several reports in prokaryotes and eukaryotes on the expression of enzymes under oxic conditions that are assigned to anaerobic metabolism (10, 23, 24). One example is the production of hydrogen by the oxygen sensitive FeFe-hydrogenase in air-grown *Chlamydomonas reinhardtii* algae in a fully aerobic environment, which is enabled by microoxic niches within the thylakoid stroma (42). Another example is the constitutive expression of PFOR and the oxygen sensitive NiFe-hydrogenase under oxic conditions in cyanobacteria. By itself, the widespread presence of these enzymes in organisms that either live predominantly aerobically as e.g. cyanobacteria or are even obligate aerobes as e.g. *Sulfolobus acidocaldarius*, which possesses a PFOR, indicates a misconception and lack of understanding. The PFOR of *Sulfolobus acidocaldarius* could be isolated as stable enzyme in the presence of O_2, however, enzyme activity measurements required the consumption of oxygen *in vitro* (11). Does this mean, that anaerobic micro-niches are required within this obligate aerobe to activate an enzyme of its central carbon metabolism? It might alternatively be that living cells have the ability to maintain reducing conditions in the presence of oxygen by yet unknown mechanisms that e.g. consume oxygen, which is a challenge in enzymatic *in vitro* assays. Conclusions on *in vivo* enzyme activities based on *in vitro* experiments therefore should be made with caution. Even though we could measure decarboxylation of pyruvate via PFOR only in the absence of oxygen *in vitro*, our data strongly indicate that this enzyme is active *in vivo* under aerobic and highly reducing conditions. We assume that either anaerobic micro-niches or alternatively mechanisms within the cell that are not understood yet, keep the enzyme active in an aerobic environment.

Low abundant ferredoxins are required for optimal photomixotrophic growth (Figure 3), which is surprising when looking at glycolytic routes for glucose oxidation. Glucose is alternatively oxidized via different glycolytic routes in *Synechocystis* (Figure 4A). Flux analyzes have shown that glycolytic intermediates enter the CBB cycle, eventually reach lower glycolysis and finally provide pyruvate (43). Depending on the precise route taken, glucose oxidation yields distinct forms of reducing equivalents (38). Three enzymes are involved in oxidation steps: Glc6P dehydrogenase (Zwf) and 6PG dehydrogenase (Gnd) yield NADPH, whereas GAP dehydrogenase

(GAPDH) yields NADH. NAD(P)H is furthermore provided downstream in the TCA cycle. PFOR is thus the only known direct source for reduced ferredoxin in glucose oxidation beside PSI (Figure 4). The wide network of low abundant ferredoxins in *Synechocystis* and the importance of these ferredoxins under photomixotrophic conditions on the one hand and the low number of known enzymes that directly reduce ferredoxins on the other hand unveils that our conception is not yet inherently consistent. An additional potential source of reduced ferredoxin could be the transfer of electrons from NAD(P)H. The transhydrogenase (PntAB), which is located in the thylakoid membrane utilizes proton translocation to transfer electrons from NADH to $NADP^+$ (44). Electrons from NADPH could be further transferred to ferredoxin via ferredoxin-NADPH-oxidoreductase (FNR). Another potential turntable for the exchange of electrons is the diaphorase part of the NiFe-hydrogenase in *Synechocystis*, which was recently shown to shuttle electrons between NAD(P)H, flavodoxin and several ferredoxins *in vitro* (29).

In order to get a complete picture of the ferredoxin network and potential interaction partners, it would be essential to know the redox potentials of all low abundant ferredoxins in *Synechocystis*. Currently, they have been determined for Fx1 (-412 mV), Fx2 (-243 mV), and Fx4 (-440 mV), whereas the value for Fx4 is based on measurements of a homologue in *Thermosynechococcus elongatus* (30, 32, 33). Fx1 to Fx6 in *Synechocystis* possess 2Fe2S clusters for which redox potentials between -240 to -440 mV are typical (5). For 3Fe4S clusters as present in Fx8 (containing one 3Fe4S and one 4Fe4S cluster) redox potentials between -120 to -430 mV were determined and for 4Fe4S clusters as present in Fx7 (4FeFS) and Fx9 (containing two 4Fe4S clusters) redox potentials between -300 to -680 mV were found (5). Our data show, that Fx9 is of importance under photomixotrophic conditions (Figure 3A). The redox potential of Fx9 in *Synechocystis* has been assumed to be around -420 mV based on its interaction partners (28). However, this value requires experimental validation. Without yet knowing the exact values for all ferredoxins in *Synechocystis*, it is obvious that they span a wide range of redox potentials. Our data indicate that cells perform a general shift from utilizing NAD(H)-dependent to ferredoxin dependent enzymes under highly reducing photomixotrophic conditions.

The following lines include theoretical reflections based on this observation. However, as these conclusions are not entirely supported by the data, they should be regarded as hypothetical and are meant as thought-provoking impulses.

The replacement of FeS enzymes and ferredoxins by FeS-free alternatives and NADPH in the course of evolution is in general discussed with regard to the oxygen sensitivity of FeS clusters in connection with the shift from anoxic to oxic conditions on Earth (8, 10). Oxygen is without any doubt one important factor. However, the shift from anoxic to oxic conditions went along with a shift from reducing to more oxidizing conditions. This shift was among others achieved by the escape of hydrogen into space, which irreversibly withdrew electrons from Earth (2). The withdrawal of electrons and the establishment of oxidizing conditions might have been an additional important factor (independent of oxygen and the oxygen sensitivity of FeS clusters) that triggered these evolutionary changes by enabling reactions with higher driving forces. The idea is thus that PFOR and ferredoxins might have been replaced by the PDH complex and NADH due to their potential to release larger amounts of Gibbs free energy ($\Delta G<0$). When competing with other organisms for resources an accelerated metabolism can be highly beneficial.

The decision to either utilize the PDH complex or alternatively PFOR and along this line, the replacement of PFOR by the PDH complex in the course of evolution might have been determined by the prioritization for high chemical driving forces.

On that note, we were unable to delete the PDH complex in *Synechocystis,* which points to its essential role. PFOR is in contrast dispensable under photoautotrophic conditions and cells obviously prefer to decarboxylate pyruvate via the PDH complex under these conditions. By transferring electrons to NAD^+ instead of ferredoxin less Gibbs free energy is stored. However, this comes along with a higher driving force that is visible when regarding the reaction Gibbs energies of $\Delta_rG'^m$ -39 kJ/mol for the reaction catalyzed by the PDH complex versus $\Delta_rG'^m$ -23 kJ/mol for the reaction catalyzed by PFOR (Figure 4C) (45).
The idea is thus that the $NADH/NAD^+$ pool gets reduced first prioritizing high driving forces. However, as the redox potential of the $NADH/NAD^+$ pool turns slowly more negative, it might reach levels that are characteristic for ferredoxin couples. This might provoke a metabolic shift to transfer electrons to oxidized ferredoxin instead of NAD^+ which should come along with lower metabolic rates (Figure 4C). This idea fits well with the observation, that PFOR and low abundant ferredoxins gain importance in the stationary growth phase (Figures 1A and 3A), which is characterized by a slowing down of metabolic reactions. The shift can be regulated on several levels. Among others, as shown in this study, high $NADH/NAD^+$ ratios can inactivate enzymes that rely on this couple and thereby support the action of isoenzymes that interact with the Fx_{red}/Fx_{ox} couple instead. In addition, a shift to more reducing conditions (Figure 1 – supplement figure 4), will alter the thermodynamic driving force of many redox reactions, and may in itself necessitate a shift in pathways. In addition, electron turntables as the transhydrogenase, FNR and the diaphorase can support this shift (29, 44).
By shifting their pools of reducing equivalents, cells are thus able to finetune their metabolism. They either liberate or save Gibbs free energy and thereby either accelerate or slow down metabolic reactions, as required.

Conclusion

The cyanobacterium *Synechocystis* encounters highly reducing conditions under photomixotrophy in the presence of oxygen. The PDH complex gets inactivated under these conditions at high $NADH/NAD^+$ ratios and is functionally most likely replaced by PFOR. PFOR is stable in the presence of oxygen *in vitro* and reduces ferredoxin instead of NAD^+. PFOR, low abundant ferredoxins and the ferredoxin-dependent GOGAT are required for optimal photomixotrophic growth and performance. Electrons from the oxidation of external glucose furthermore rely upon the presence of photosynthetic complex I (which accepts electrons from ferredoxin) in order to reach PSI. These findings indicate that cells perform a general shift in the utilization of their reducing equivalent pools from NAD(H) to ferredoxin under photomixotrophic conditions.

Materials and Methods

Bioinformatic analysis concerning the distribution of PFOR and PDH complex in cyanobacteria
All completely sequenced cyanobacterial genomes were analyzed via tblastn for the presence of the PDH complex and PFOR. For this, in order to exclude symbionts, cyanobacterial genomes were in a first step searched for the *psbD* gene (PSII subunit). We used the *psbD* gene (*sll0849*) of *Synechcoystis* as bait. Only genomes containing *psaD* were used for all further analysis. 197 genomes remained and were searched by tblastn using the *pdhA* subunit (*slr1934*) from the PDH complex from *Synechcoystis* as bait. The largest expect value was $2x10^{-136}$. *pdhA* was found in all genomes analyzed. 67 of these genomes contain *nifD* (highest e-value $4x10^{-104}$) and *nifK* (highest e-value $1x10^{-73}$), the two subunits of the nitrogenase for N_2-fixation and a diazotrophic lifestyle.

Diazotrophic and non-diazotrophic cyanobacteria were searched for the presence of PFOR by using *sll0741* from *Synechcoystis*. The highest e-value in this case was 0.

Growth conditions

All strains were grown in 50 ml BG-11 (46) buffered with TES pH 8. WT, Δ*pfor*, Δ*f-gogat*, Δ*n-gogat*, Δ*isiB*, all ferredoxin deletion mutants, Δ*ndhD1*Δ*ndhD2*, Δ*hk*, and Δ*glgP1*Δ*glgP2* were and placed in 100 ml Erlenmeyer flasks on a rotary shaker at 28 °C, 50 µE m^{-2} s^{-1} and 100 rpm. After several days of growth, the cells were inoculated into 200 ml BG-11 at an OD_{750} of 0.05 and placed into glass tubes bubbled with air at 50 µE m^{-2} s^{-1} at 28 °C and growth was monitored by measuring the optical density at 750 nm. In liquid cultures all the strains were grown without addition of antibiotics and for photomixotrophic conditions 10 mM glucose was added.
For mutant selection and seggregation the cells were grown on BG-11-agar containing 50 µg/mL kanamycin, 20 µg/mL spectinomycin, 25 µg/mL erythromycin, 10 µg/mL gentamycin, and 20 µg/mL chloramphenicol.

Construction of mutants

All the primers used in this study are listed in Supplementary File 1a. All mutants are listed in Supplementary File 1a. All mutants were constructed in the non-motile GT WT of *Synechocystis* sp. PCC 6803 (47). The procedure to generate the constructs for deletion of *pfor*, *pdhA*, *isiB* and the different ferredoxin genes was described in Hoffmann et al. (2006) (48). In brief, the up- and downstream regions as well as the required antibiotic resistance cassette were amplified by PCR. Subsequently, the three fragments were combined by a PCR fusion including the outermost primers. The resulting product was inserted by TA-cloning into the pCR2.1 TOPO-vector (ThermoFisher, Waltham, MA, USA). Constructs for the deletion of the genes of the NADH-dependent and the ferredoxin-dependent GOGAT were generated by Gibson cloning (49) assembling three fragments into the pBluescript SK(+) in a single step. After examination by sequencing the plasmids were transformed into *Synechocystis* sp. PCC 6803 cells as described (50). Resulting transformants were either checked by PCR or Southern hybridization after several rounds of segregation (Fig. S7).To generate a construct for overexpression of *pfor* (*sll0741*) including a His-tag a DNA fragment containing 212 bp up- and 212 bp downstream of the *sll0741* start codon, with a BamHI, XhoI and NdeI site in between and 20 bp sequences that overlap with the pBluescript SK(+) vector at the respective ends was synthesized by GeneScript (Psicataway Township, NJ, USA)(Fig S4). Another DNA fragment containing a modified petE promotor, followed by His-tag, TEV cleavage recognition site and linker encoding sequences, various restriction sites and 20 bp sequences that overlap with the pBluescript SK(+) vector at the respective ends was also synthesized by GenScript. These fragments were cloned into the pBluescript SK(+) vector by Gibson cloning, respectively. A kanamycin antibiotic resistance cassette was inserted into the EcoRV site of the plasmid containing the modified petE promotor. The resulting promoter-cassette plasmid and the PFOR plasmid were digested with BamHI and NdeI and the promoter cassette was ligated into the alkaline phosphatase treated PFOR plasmid to yield the final construct. This plasmid was sequenced, transformed into *Synechocystsis* sp. PCC 6803 and segregation was confirmed by PCR analysis (Figure 3 – figure supplement 1).

Southern-Blotting

200 ng genomic DNA was digested with Hind III and loaded on a 0.8 % agarose gel in TBE buffer. After blotting the DNA on a nylon membrane (Hybond N+, Merck, Darmstadt, Germany) it was cross-linked to the membrane in a Stratalinker (Stratagene, CA, USA). Detection of the respective bands was carried out by the Dig DNA labeling and detection kit (Roche, Penzberg, Germany) according to the manufacturer´s instructions.

RT-PCR

To a volume of 15 µl containing 1 µg of RNA 2 µl RNase-free DNase (10 U/µl, MBI Fermentas, St. Leon-Rot, Germany), 2 µl 10 x DNase buffer (MBI Fermentas, St. Leon-Rot, Germany) and 1 µl Riboblock RNase Inhibitor (40 U/µl, MBI Fermentas, St. Leon-Rot, Germany) were added before incubation at 37 °C for 2 hours. Subsequently the sample was quickly cooled on ice. 2 µl 50 mM EDTA was added and it was incubated at 65 °C for 10 min and again quickly cooled on ice to get rid of the DNase activity. To check the digestion efficiency, 1 µl of the sample was used as a template for PCR. 1 µl genomic DNA and 1 µl H_2O were used as positive and negative controls, respectively. Reverse transcription PCR was performed with 9 µl of those samples free of DNA with the RT-PCR kit (Applied Biosystems, Karlsruhe, Germany) according to the manufacturer's instruction. 9 µl of the same sample was used in parallel as a negative control. The reaction mixture was incubated for 1 h at 37 °C including a gene-specific tag-1 primer. For the subsequent PCR a gene-specific tag-2 primer and the respective reverse primer (see Supplementary File 1a) were used.

Oxygen measurements

To measure the concentration of dissolved oxygen in the cultures, oxygen sensors from Unisense (Unisense, Aarhus, Denmark) were used. After a two-point calibration of the sensor by using distilled water equilibrated with air and a solution with 0.1 M NaOH and 0.1 M ascorbate containing no oxygen it was placed in the respective culture and the measurement was started.

Determination of NAD^+/NADH

All the cultures used for NAD^+/NADH determination experiment were grown autotrophically and mixotrophically in 250 ml BG-11 medium. 5 ml to 10 ml cells, equivalent to about 10^9 cells/ml (10 ml cultures of OD_{750} of 1) were sampled for the measurements. The cells were centrifuged at 3,500 x g -9 °C for 10 min and the pellets were washed with 1 ml 20 mM cold PBS (20 mM KH2PO4, 20 mM K2HPO4, and 150 mM NaCl). The suspension was transferred to a 2 ml reaction cup and was centrifuged at 12,000 x g for 1 min at -9 °C. For all further steps the NAD+/NADH Quantification Colorimetric Kit (Biovision, CA, USA) was used. The pellet was resuspended in 50 µl extraction buffer and precooled glass beads (Ø=0.18 mm) were added to about 1 mm to the surface of the liquid. The mixture was vortexed 4 times 1 min in the cold room (4 °C) and intermittently chilled on the ice for 1 min. 150 µl extraction buffer was added again and the mixture was centrifuged at 3,500 xg for 10 min at -9 °C. The liquid phase was transferred as much as possible into a new reaction cup and centrifuged at maximum speed for 30 min at -9 °C. All further steps were conducted as described by the manufacturer. Finally, the samples were incubated for 1 to 4 hours in 96 well plates before measuring absorbance at 450 nm by TECAN GENios (TECAN Group Ltd., Austria) along with a NADH standard curve.

Determination of the redox level of ferredoxin

To compare the redox level of the ferredoxin pool of autotrophic and mixotrophic WT cells the Dual-KLAS/NIR was used (51). Cells were grown for three days under either conditions, harvested and adjusted to 20 µg chlorophyll/ml for the measurements. The cell suspension was consecutively illuminated with increasing light intensities between 35 and 162 µE/m^2/s. At lower light intensities the signal was notoriously noisy and not used further. Each new light intensity was applied to the cells for one minute to reach steady state before data acquisition started. To this end a multiple turnover pulse of 800 ms and 19,800 µE/m^2/s was applied six times every 24 s on top of the actinic light intensity to fully oxidize or reduce the respective component. The averaged data recorded just before, during and after the pulse was used to determine the signal height for all three redox partners (P700, plastocyanin and ferredoxin). This signal was divided by the maximal signal recorded by a NirMax measurement done with the same sample as described before (36). Under steady state conditions the FeS-signal detected by the Dual-KLAS/NIR should be close to the redox state of ferredoxin since the FeS clusters of PSI should be in equilibrium with those in ferredoxin.

Determination of the redox level of NAD(P)H

To compare the redox level of NAD(P)H of autotrophic and mixotrophic WT cells the Dual-KLAS/NIR was connected to the NADPH-module (51). Cells from three days old cultures were harvested and adjusted to 10 µg chlorophyll/ml for measurement. The cell suspension was consecutively illuminated with increasing light intensities between 16 and 162 µE/m^2/s. Each new light intensity was applied to the cells for one minute to reach steady state before data acquisition started. In this case a two second pulse of 740 µE/m^2/s was applied 10 times every 13 s on top of the actinic light intensity to fully reduce NAD(P)H. The data was recorded from about four seconds before the pulse to four seconds after the pulse with an average over 50 data points. After averaging all ten measurements the signal height was determined to get an estimate on how much NAD(P)H could still be reduced. In parallel to these measurements the oxygen evolution was measured by an oxygen microelectrode (Unisense, Aarhus, Denmark) to determine the amount of electrons available for $NADP^+$ reduction due to linear electron transport.

Purification and activity measurement of dihydrolipoyl dehydrogenase (E3 subunit, SynLPD)

The recombinant His-tagged SynLPD (Slr1096) was generated and purified essentially as described previously (52). Prior activity measurements, the elution fractions were desalted through PD10 columns (GE healthcare, Solingen, Germany). The protein concentration was determined according to Bradford (53). SynLPD activity was determined in the forward direction. DL-dihydrolipoic acid served as the substrate at a final concentration of 3 mM. SynLPD activity was followed as reduction of NAD^+ (included in varying concentrations, 0.1, 0.2, 0.3, 0.4, 0.5, 1, 2, 3, 4 and 5 mM) at 340 nm. The K_i constant was estimated in the presence of four NADH concentrations (0, 0.1, 0.15 and 0.2 mM) as well as NADPH (0.1 mM) as control. Specific enzyme activity is expressed in µmol NADH per min^{-1} mg $protein^{-1}$ at 25°C. Mean values and standard deviations were calculated from at least three technical replicates for all substrate/co-substrate combinations. All chemicals were purchased from Merck (Darmstadt, Germany).

Purification of pyruvate:ferredoxin oxidoreductase (PFOR)

For the purification of PFOR from *Synechocystis* sp. PCC 6803 (Fig. S6), three 6-L autotrophic cultures of the PFOR overexpression strain (PFOR:oe) were grown to an OD_{750} of about 1. Cells

were harvested by centrifugation at 4.000 rpm in a JLA-8.1000 rotor for 20 min at 4°C. Initially, His-PFOR over-expression in the 6-L cultures was assessed by SDS PAGE analysis followed by immunoblotting with a His-tag specific antibody (GenScript; Fig S4). A specific band could be detected in the over-expression mutant, confirming expression and stable accumulation of the over-expressed and N-terminally His-tagged PFOR protein. For large-scale purification cells were resuspended in lysis buffer (50 mM $NaPO_4$ pH=7.0; 250 mM NaCl; 1 tablet complete protease inhibitor EDTA free (Roche, Basel, Switzerland) per 50 mL) and broken by passing them through a French Press cell at 1250 p.s.i. twice. Unbroken cells and membranes were pelleted in a Beckman ultracentrifuge using a 70 Ti rotor at 35.000 rpm for 45 min at 4°C. The decanted soluble extract was adjusted to a volume of 90 mL with lysis buffer and incubated with 10 mL TALON cobalt resin (Takara, Shiga, Japan) for 1 h at 4°C. The resin was then washed extensively with 200 mL lysis buffer and subsequently with 100 mL lysis buffer containing 5 mM imidazole. Bound proteins were eluted with 20 mL elution buffer (50 mM $NaPO_4$ pH=7.0; 250 mM NaCl; 500 mM imidazole). The protein was concentrated overnight to a volume of 2 mL in a Vivaspin 20 Ultrafiltration Unit (5 kDa MWCO)(Merck, Darmstadt, Germany) and then loaded onto a HiLoad^{TM} 26/60 Superdex TM 75 prep grade (GE Healthcare, Chicago, IL, USA) using 25 mM $NaPO_4$, pH=7.0; 50 mM NaCl; 5% (v/v) glycerol as the running buffer. The run was monitored at 280 nm and fractions were collected (Fig. 5A).

Acitivity measurement of pyruvate:ferredoxin oxidoreductase (PFOR)

The specific activity of the pyruvate:ferredoxin oxidoreductase was measured essentially as described (11). The activity assay contained in 1 ml 100 mM Tris-HCl (pH 8), 0.5 mM Coenzyme A, 10 mM pyruvate, 5 mM thiamine pyrophosphate, 40 mM glucose, 40 U glucose oxidase, 50 U catalase, and 10 mM methy viologen. Reduction of methylviologen was followed at 604 nm and an extinction coefficient of 13.6 mM^{-1} cm^{-1} was used. The reaction was started by adding 8.9 x 10^{-5} M isolated PFOR.

We also tested ferredoxin reduction by the PFOR by a mixture containing the same substances as above except methyl viologen. To this mixture 1.6 mM ferredoxin 1 and 1.3 mM ferredoxin:$NADP^+$ reductase and 1 mM $NADP^+$ were added. In this case the reduction of $NADP^+$ was followed at 340 nm. The same mixture without glucose, glucose oxidase and catalase were used to test if the enzyme also works in the presence of oxygen.

In-vivo electron flow through photosystem I

The electron flux through photosystem I was measured by the Dual-KLAS/NIR (Walz GmbH, Effeltrich, Germany) by a newly developed method (36). In brief, cell suspensions were adjusted to 20 µg/mL chlorophyll and 20 µM DCMU was added. Electron flow through PSI was determined by dark-interval relaxation kinetics (DIRK) measurements at a light intensity of 168 $\mu E/m^2/s$ in the absence and presence of 10 mM glucose.

Determination of reaction Gibbs energies

$\Delta_r G'^m$ for the reaction catalyzed by the PDH complex and by PFOR were calculated using eQuilibrator (http://eauilibrator.weizmann.ac.il/) according to (45). CO_2 (total) was considered as hydrated and dehydrated forms of CO_2 are considered to be in equilibrium in biochemical reactions. Ionic strength of 0.2M, pH of 7 and metabolite concentrations of 1 mM were assumed. In order to determine the redox potential of pyruvate we used the reactions Gibbs energy of -39 kJ/mol for the PDH complex and -23 kJ/mol for PFOR. Assuming a redox potential

of -320 mV for NAD(P)H and -400 mV for ferredoxin the potential of pyruvate was determined according to $\Delta G = -nF\Delta E$ to -520 mV.

Figure legends:

Figure 1: (A) Growth and (B) $NADH/NAD^+$ ratios of wild type (WT) and Δ*pfor* under photoautotrophic and photomixotrophic (+ glc) conditions in continuous light. Shown are mean values ± SD from at least 3 replicates.

Figure 1 – figure supplement 1: Bioinformatic analyses concerning the distribution of PDH complex and PFOR in diazotrophic and non-diazotrophic cyanobacteria. All shown genomes possess a PDH complex.

Figure 1 – figure supplement 2: Oxygen concentrations in photomixotrophic cultures of wild type (WT) and Δ*pfor* were close to oxygen saturation throughout the growth experiments. Original traces are shown.

Figure 1 – figure supplement 3: RT-PCR showing that *pfor* and *pdhA* are transcribed under photoautotrophic and photomixotrophic conditions in the wild type. Total RNA of wild type cells was reverse transcribed and subsequently subjected to PCRs with either primers specific for *rnpB*, *pfor* or *pdhA* (Supplementary File 1a). In the control reactions (C) reverse transcriptase was omitted.

Figure 1 – figure supplement 4: Redox states of NAD(P)H and ferredoxin and O_2-turnover in auto- and mixotrophic cultures. A: NAD(P)H fluorescence measurements were applied to get an estimate of its redox state under photomixotrophic in comparison to photoautotrophic conditions *in vivo*. This method does not distinguish between NADPH and NADH, though. The reduction level of NAD(P)H was determined by applying a strong light pulse (740 $\mu E/m^2/s$) in addition to actinic light (0-160 $\mu E/m^2/s$). The resulting signal differences give an estimate about the amount of available $NAD(P)^+$, which can still be reduced. Low NAD(P)H signals thus indicate a rather reduced NAD(P)H pool, as shown for photomixotrophic in comparison to photoautotrophic conditions. B: The reduction level of the ferredoxin pool was determined using the Dual-KLAS/NIR. The ferredoxin pool which was likewise more reduced under photomixotrophy C: Oxygen evolution was determined in parallel and found that it was reduced to about half of that of the photoautotrophic ones. Thus, linear electron transport should still be able to reduce about half of the NAD(P)H compared to photoautotrophic cultures. Thus, since NAD(P)H is barely reducibly under photomixotrophy these data clearly show, that the NAD(P)H pool is strongly reduced in the presence of glucose. This is well in line with the $NADH/NAD^+$ levels that are likewise rather reduced under photomixotrophy (Figure 1B).

Figure 2: (A) Inhibition of the PDH complex in *Synechocystis* via inactivation of the dihydrolipoyl dehydrogenase (E3) subunit (SynLPD) by NADH. I: The rate of recombinant SynLPD activity (3

mM DL-dihydrolipoic acid) as a function of NAD^+ (0.1, 0.2, 0.3, 0.4, 0.5, 1, 2, 3, 4 and 5 mM) reduction in the presence of the indicated NADH concentrations (0, 0.1, 0.15 and 0.2 mM). NADPH (0.1 mM) was used as a control to demonstrate the specificity of NADH inhibition. Specific enzyme activity is expressed in µmol NADH per min^{-1} mg $protein^{-1}$ at 25ºC. II: Lineweaver-Burk plots of enzyme activities at four NADH concentrations. III: The inhibitor constant (K_i) was estimated by linear regression of (I) the slopes of the three Lineweaver-Burk plots at the four NADH concentrations versus (II) the NADH concentration. Shown are mean values ± SD from at least 3 technical replicates. (B) Enzyme activity of PFOR that was purified in the presence of oxygen. PFOR activity was measured in the presence of FNR, ferredoxin and $NADP^+$. The reaction was started by addition of 10 mM pyruvate as indicated by the arrow. Assay 1 (blue line): The assay mixture was kept anaerobic with 40 mM glucose, 40 U glucose oxidase and 50 U catalase, showing that PFOR, which was purified in the presence of oxygen, is active. Assay 2 (red line): Assay 2 had the same composition as assay 1 but glucose, glucose oxidase and catalase were omitted, showing that anaerobic conditions are required for activity of PFOR *in vitro*. Assay 3 (grey line): This assay is the continuation of the measurement of assay 2 after addition of glucose, glucose oxidase and catalase. Representative traces of three replicates are shown.

Figure 2 – figure supplement 1: SDS PAGE analysis followed by immunoblotting of *Synechocystis* soluble extracts. Soluble extracts for the wild type (WT) and the mutant overexpressing PFOR (PFOR:oe) containing 15 µg of protein were loaded per lane. The arrowhead indicates the position of over-expressed PFOR.

Figure 2 – figure supplement 2: Large-scale PFOR purification. (A) The chromatogram of the FPLC size exclusion run. The collected fractions (5 to 7) are marked by the black bar underneath. (B) Various fractions from the purification procedure were analyzed by SDS PAGE. Soluble extracts before (Pre) and after (Post) the incubation with Talon Cobalt resin, a wash fraction, the His-tag elution and the pooled FPLC fraction (5 t to 7) were loaded on the gel.

Figure 2 – figure supplement 3: PCR analysis of PFOR overexpression (pfor:oe) mutant and WT.

Figure 3: (A) Photomixotrophic growth of wild type (WT), Δ*pfor*, ferredoxin (fx) and flavodoxin (isiB) deletion mutants as indicated. (B) Growth of WT, Δ*f-gogat* and Δ*n-gogat* under photoautotrophic and photomixotrophic conditions. (C) Electron transport with DCMU at PSI in the absence and presence of glucose in the WT, Δ*ndhD1*Δ*ndhD2*, Δ*hk* and ΔglgP1Δ*glgP2*. Shown are mean values ± SD from at least 3 replicates.

Figure 3 – figure supplement 1: Examination of segregation of mutant strains. (A) PCR analysis of WT, ferredoxin (fx) and flavodoxin (isiB) mutants as indicated. (B) Southern blot of WT and Δ*n-gogat* and Δ*f-gogat* deletion mutants. WT DNA and DNA of two different mutant clones were applied after HindIII digestion. The sizes of the bands are indicated and correspond to those expected due to the mutation.

Figure 3 – figure supplement 2: Photoautotrophic growth of different ferredoxin (fx) and the flavodoxin (isiB) deletion mutant as indicated in comparison to the wild type (WT). Shown are mean values ± SD from at least 3 replicates.

Figure 4: Optimal photomixotrophic growth requires low abundant ferredoxins, PFOR and F-GOGAT. Electrons from glucose oxidation that arrive at PSI require ferredoxin-dependent photosynthetic complex I (NDH-1). Cells shift from utilizing NAD(H) dependent to ferredoxin dependent enzymes when brought from photoautotrophic to photomixotrophic conditions. (A) Glycolytic routes, lower glycolysis and the TCA cycle yield NAD(P)H from glucose oxidation. The only known enzyme that produces reduced ferredoxin from glucose oxidation is PFOR. Both the decarboxylation of pyruvate as well as the synthesis from glutamate from 2-oxoglutarate and glutamine can be catalyzed by distinct enzymes that either utilize ferredoxin (PFOR, F-GOGAT) or NAD(H) (PDH-complex; N-GOGAT). (B) Photosynthetic complex I (NDH-1) accepts electrons from reduced ferredoxin. The complex is required for the input of electrons from glucose oxidation into photosynthesis in the presence of DCMU. (C) The $\Delta_rG'^m$ of pyruvate decarboxylation via the PDH complex is more negative that via PFOR, which results in a higher driving force (for calculations see materials and methods part). Photomixotrophy results in reducing conditions. The redox potential of the NAD(P)H/NAD(P)$^+$ pool which is around -320 mV will turn more negative upon reduction. This could facilitate the transfer of electrons from NADH to ferredoxins. In addition, inactivation of NAD$^+$ dependent enzymes (such as the PDH complex) and their functional replacement by ferredoxin dependent enzymes (such as PFOR) support the suggested shift from the utilization of the NAD(H) to the ferredoxin pool.

Figure 1 – source data: Raw data of growth and NADH/NAD$^+$ ratio of WT and Δpfor under photoautotrophic and photomixotrophic conditions

Figure 1 – figure supplement 1 – source data: Raw data of bioinformatic analysis of the occurrence of PFOR and the PDH complex in cyanobacteria

Figure 1 – figure supplement 2 – source data: Raw data of oxygen concentration in photomixotrophic WT and Δpfor cultures

Figure 1 – figure supplement 3 – source data: Uncropped raw gel of RT-PCR

Figure 2 – source data: Raw data of enzymatic in vitro test with the dihydrolipoyl dehydrogenase (E3) subunit (SynLPD) of the PDH complex and PFOR

Figure 2 – figure supplement 1 – source data: Uncropped gel and blot of overexpression of PFOR (PFOR:oe)

Figure 2 – figure supplement 2 – source data: Uncropped gel of PFOR purification

Figure 3 – source data: Raw data from growth of WT, Δ*pfor*, Δfx, ΔisiB, Δ*f-gogat* and Δ*n-gogat* and electron transport with DCMU at PSI in the absence and presence of glucose in the WT, Δ*ndhD1*Δ*ndhD2*, Δ*hk* and ΔglgP1Δ*glgP2*.

Figure 3 - figure supplement 1 - source data: Uncropped raw gels and blots from the examination of deletion mutants

Figure 3 - figure supplement 2 - source data: Raw data from photoautotrophic growth of different ferredoxin (fx) and the flavodoxin (isiB) deletion mutant as indicated in comparison to the wild type (WT).

Supplementary File 1a: List of primers used in this study to generate deletion strains and for RT-PCR.

Supplementary File 1b: Liste of *Synechocystis* strains and mutants used in this study.

Acknowledgments

This study was supported by grants from the China Scholarship Council (CSC) (Grant # 201406320187), FAZIT-Stiftung, Deutsche Bundesstiftung Umwelt, German Ministry of Science and Education (BMBF FP309), and the German Science Foundation (DFG Gu1522/2-1, HA2002/23-1 and FOR2816).

References

1. K. J. Zahnle, D. C. Catling, M. W. Claire, The rise of oxygen and the hydrogen hourglass. *Chemical Geology* **362**, 26-34 (2013).
2. D. C. Catling, K. J. Zahnle, C. P. McKay, Biogenic Methane, Hydrogen Escape, and the Irreversible Oxidation of Early Earth. *Science* **293**, 839 (2001).
3. M. J. Russell, W. Martin, The rocky roots of the acetyl-CoA pathway. *Trends in Biochemical Sciences* **29**, 358-363 (2004).
4. G. Wächtershäuser, Evolution of the first metabolic cycles. *Proceedings of the National Academy of Sciences* **87**, 200 (1990).
5. J. Liu *et al.*, Metalloproteins Containing Cytochrome, Iron–Sulfur, or Copper Redox Centers. *Chemical Reviews* **114**, 4366-4469 (2014).
6. J. D. Kim, A. Rodriguez-Granillo, D. A. Case, V. Nanda, P. G. Falkowski, Energetic Selection of Topology in Ferredoxins. *PLoS Comput Biol* **8**, e1002463 (2012).
7. M. Müller *et al.*, Biochemistry and Evolution of Anaerobic Energy Metabolism in Eukaryotes. *Microbiology and Molecular Biology Reviews* **76**, 444 (2012).
8. J. A. Imlay, Iron-sulphur clusters and the problem with oxygen. *Molecular Microbiology* **59**, 1073-1082 (2006).
9. B. Jagannathan, G. Shen, J. Golbeck, The evolution of type I reaction centers: the response to oxygenic photosynthesis. *Advances in Photosynthesis and Respiration* **33** (2012).
10. S. B. Gould *et al.*, Adaptation to life on land at high O2 via transition from ferredoxin-to NADH-dependent redox balance. *Proceedings of the Royal Society B: Biological Sciences* **286**, 20191491 (2019).
11. A. Witt, R. Pozzi, S. Diesch, O. Hädicke, H. Grammel, New light on ancient enzymes – in vitro CO2 Fixation by Pyruvate Synthase of Desulfovibrio africanus and Sulfolobus acidocaldarius. *The FEBS Journal* **286**, 4494-4508 (2019).
12. A. Mall *et al.*, Reversibility of citrate synthase allows autotrophic growth of a thermophilic bacterium. *Science* **359**, 563 (2018).

13. M. C. Evans, B. B. Buchanan, D. I. Arnon, A new ferredoxin-dependent carbon reduction cycle in a photosynthetic bacterium. *Proceedings of the National Academy of Sciences of the United States of America* **55**, 928-934 (1966).
14. K. Gutekunst, Hypothesis on the Synchronistic Evolution of Autotrophy and Heterotrophy. *Trends in Biochemical Sciences* **43**, 402-411 (2018).
15. G. Fuchs, Alternative Pathways of Carbon Dioxide Fixation: Insights into the Early Evolution of Life? *Annual Review of Microbiology* **65**, 631-658 (2011).
16. L. Pieulle *et al.*, Isolation and characterization of the pyruvate-ferredoxin oxidoreductase from the sulfate-reducing bacterium Desulfovibrio africanus *Biochimica Et Biophysica Acta-Protein Structure and Molecular Enzymology* **1250**, 49-59 (1995).
17. L. Pieulle, V. Magro, E. C. Hatchikian, Isolation and analysis of the gene encoding the pyruvate-ferredoxin oxidoreductase of Desulfovibrio africanus, production of the recombinant enzyme in Escherichia coli, and effect of carboxy-terminal deletions on its stability. *Journal of Bacteriology* **179**, 5684-5692 (1997).
18. N. Vita, E. C. Hatchikian, M. Nouailler, A. Dolla, L. Pieulle, Disulfide Bond-Dependent Mechanism of Protection against Oxidative Stress in Pyruvate-Ferredoxin Oxidoreductase of Anaerobic Desulfovibrio Bacteria. *Biochemistry* **47**, 957-964 (2007).
19. L. Kerscher, D. Oesterhelt, Purification and Properties of Two 2-Oxoacid:Ferredoxin Oxidoreductases from Halobacterium halobium. *European Journal of Biochemistry* **116**, 587-594 (1981).
20. L. Kerscher, D. Oesterhelt, Ferredoxin is the coenzyme of alpha-ketoacid oxidoreductases in Halobacterium halobium. *FEBS Lett* **83**, 197-201 (1977).
21. S. Li *et al.*, Dynamic control over feedback regulatory mechanisms improves NADPH flux and xylitol biosynthesis in engineered E. coli. *Metab Eng* **64**, 26-40 (2021).
22. T. Nakayama, S. Yonekura, S. Yonei, Q. M. Zhang-Akiyama, Escherichia coli pyruvate:flavodoxin oxidoreductase, YdbK - regulation of expression and biological roles in protection against oxidative stress. *Genes Genet Syst* **88**, 175-188 (2013).
23. O. Schmitz, J. Gurke, H. Bothe, Molecular evidence for the aerobic expression of nifJ, encoding pyruvate : ferredoxin oxidoreductase, in cyanobacteria. *FEMS Microbiol. Lett.* **195**, 97-102 (2001).
24. K. Gutekunst *et al.*, LexA regulates the bidirectional hydrogenase in the cyanobacterium Synechocystis sp. PCC 6803 as a transcription activator. *Molecular Microbiology* **58**, 810-823 (2005).
25. Y. Kim, L. O. Ingram, K. T. Shanmugam, Dihydrolipoamide Dehydrogenase Mutation Alters the NADH Sensitivity of Pyruvate Dehydrogenase Complex of Escherichia coli K-12. *Journal of Bacteriology* **190**, 3851-3858 (2008).
26. Z. Sun *et al.*, Amino acid substitutions at glutamate-354 in dihydrolipoamide dehydrogenase of Escherichia coli lower the sensitivity of pyruvate dehydrogenase to NADH. *Microbiology* **158**, 1350-1358 (2012).
27. E. Kolobova, A. Tuganova, I. Boulatnikov, K. M. Popov, Regulation of pyruvate dehydrogenase activity through phosphorylation at multiple sites. *Biochem. J.* **358**, 69-77 (2001).
28. C. Cassier-Chauvat, F. Chauvat, Function and Regulation of Ferredoxins in the Cyanobacterium Synechocystis PCC6803: Recent Advances. *Life* **4**, 666-680 (2014).

29. J. H. Artz *et al.*, The structure and reactivity of the HoxEFU complex from the cyanobacterium Synechocystis sp. PCC 6803. *Journal of Biological Chemistry* 10.1074/jbc.RA120.013136 (2020).
30. H. Bottin, B. Lagoutte, Ferrodoxin and flavodoxin from the cyanobacterium Synechocystis sp PCC 6803. *Biochimica et Biophysica Acta (BBA) - Bioenergetics* **1101**, 48-56 (1992).
31. K. Gutekunst *et al.*, The Bidirectional NiFe-hydrogenase in Synechocystis sp. PCC 6803 Is Reduced by Flavodoxin and Ferredoxin and Is Essential under Mixotrophic, Nitrate-limiting Conditions. *Journal of Biological Chemistry* **289**, 1930-1937 (2014).
32. M. Schorsch *et al.*, A unique ferredoxin acts as a player in the low-iron response of photosynthetic organisms. *Proceedings of the National Academy of Sciences* **115**, E12111 (2018).
33. T. Motomura *et al.*, An alternative plant-like cyanobacterial ferredoxin with unprecedented structural and functional properties. *Biochimica et Biophysica Acta (BBA) - Bioenergetics* **1860**, 148084 (2019).
34. H. Mustila, Y. Allahverdiyeva, J. Isojärvi, E. M. Aro, M. Eisenhut, The bacterial-type [4Fe–4S] ferredoxin 7 has a regulatory function under photooxidative stress conditions in the cyanobacterium Synechocystis sp. PCC 6803. *Biochimica et Biophysica Acta (BBA) - Bioenergetics* **1837**, 1293-1304 (2014).
35. J. M. Schuller *et al.*, Structural adaptations of photosynthetic complex I enable ferredoxin-dependent electron transfer. *Science* **363**, 257-260 (2019).
36. M. L. Theune *et al.*, In-vivo quantification of electron flow through photosystem I – Cyclic electron transport makes up about 35% in a cyanobacterium. *Biochimica et Biophysica Acta (BBA) - Bioenergetics* **1862**, 148353 (2021).
37. S. Doello, A. Klotz, A. Makowka, K. Gutekunst, K. Forchhammer, A specific glycogen mobilization strategy enables awakening of dormant cyanobacteria from chlorosis. *Plant Physiology* **177**, 594-603 (2018).
38. A. Makowka *et al.*, Glycolytic Shunts Replenish the Calvin–Benson–Bassham Cycle as Anaplerotic Reactions in Cyanobacteria. *Molecular Plant* **13**, 471-482 (2020).
39. H. Ohkawa, H. B. Pakrasi, T. Ogawa, Two types of functionally distinct NAD(P)H dehydrogenases in Synechocystis sp. strain PCC6803. *J Biol Chem* **275**, 31630-31634 (2000).
40. H. P. Blaschkowski, J. Knappe, M. Ludwig-Festl, G. Neuer, Routes of Flavodoxin and Ferredoxin Reduction in Escherichia coli. *European Journal of Biochemistry* **123**, 563-569 (1982).
41. Q. Wang, M. S. Ou, Y. Kim, L. O. Ingram, K. T. Shanmugam, Metabolic Flux Control at the Pyruvate Node in an Anaerobic Escherichia coli Strain with an Active Pyruvate Dehydrogenase. *Applied and Environmental Microbiology* **76**, 2107-2114 (2010).
42. O. Liran *et al.*, Microoxic Niches within the Thylakoid Stroma of Air-Grown Chlamydomonas reinhardtii Protect [FeFe]-Hydrogenase and Support Hydrogen Production under Fully Aerobic Environment. *Plant Physiology* **172**, 264-271 (2016).
43. T. Nakajima *et al.*, Integrated Metabolic Flux and Omics Analysis of Synechocystis sp. PCC 6803 under Mixotrophic and Photoheterotrophic Conditions. *Plant and Cell Physiology* **55**, 1605-1612 (2014).

44. J. Kämäräinen *et al.*, Pyridine nucleotide transhydrogenase PntAB is essential for optimal growth and photosynthetic integrity under low-light mixotrophic conditions in Synechocystis sp. PCC 6803. *New Phytologist* 10.1111/nph.14353, n/a-n/a (2016).
45. E. Noor, H. S. Haraldsdóttir, R. Milo, R. M. T. Fleming, Consistent Estimation of Gibbs Energy Using Component Contributions. *PLOS Computational Biology* **9**, e1003098 (2013).
46. R. Rippka, J. Deruelles, J. B. Waterbury, M. Herdman, R. Y. Stanier, Generic Assignments, Strain Histories and Properties of Pure Cultures of Cyanobacteria. *Journal of General Microbiology* **111**, 1-61 (1979).
47. D. Trautmann, B. Voss, A. Wilde, S. Al-Babili, W. R. Hess, Microevolution in cyanobacteria: re-sequencing a motile substrain of Synechocystis sp. PCC 6803. *DNA Res* **19**, 435-448 (2012).
48. D. Hoffmann, K. Gutekunst, M. Klissenbauer, R. Schulz-Friedrich, J. Appel, Mutagenesis of hydrogenase accessory genes of Synechocystis sp. PCC 6803. *FEBS Journal* **273**, 4516-4527 (2006).
49. D. G. Gibson *et al.*, Enzymatic assembly of DNA molecules up to several hundred kilobases. *Nature Methods* **6**, 343-345 (2009).
50. J. G. K. Williams, "Construction of specific mutations in photosystem II photosynthetic reaction center by genetic engineering methods in Synechocystis 6803" in Methods in Enzymology. (Academic Press, 1988), vol. 167, pp. 766-778.
51. C. Klughammer, U. Schreiber, Deconvolution of ferredoxin, plastocyanin, and P700 transmittance changes in intact leaves with a new type of kinetic LED array spectrophotometer. *Photosynthesis Research* **128**, 195-214 (2016).
52. O. Reinholdt *et al.*, Redox-Regulation of Photorespiration through Mitochondrial Thioredoxin o1. *Plant Physiology* **181**, 442 (2019).
53. M. M. Bradford, A rapid and sensitive method for the quantitation of microgram quantities of protein utilizing the principle of protein-dye binding. *Analytical Biochemistry* **72**, 248-254 (1976).

Figure 1

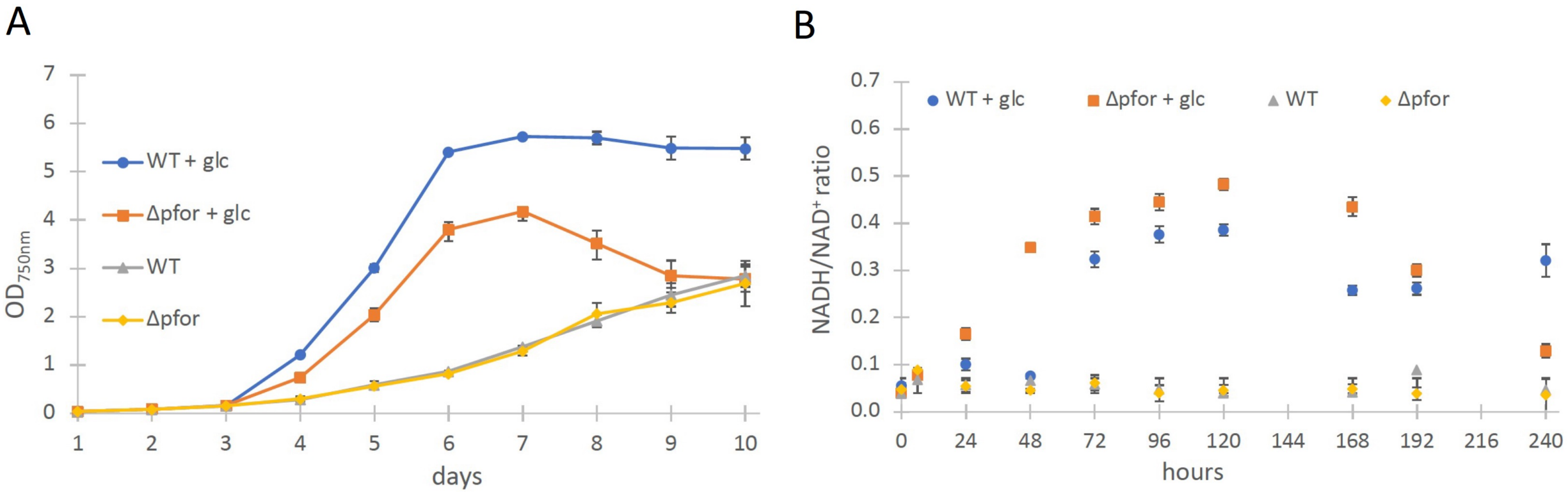
A
B
WT + glc
Δpfor + glc
WT
Δpfor
OD750nm
days
NADH/NAD+ ratio
hours
0
1
2
3
4
5
6
7
0.0
0.1
0.2
0.3
0.4
0.5
0.6
0.7
24
48
72
96
120
144
168
192
216
240

Figure 1- figure supplement 1

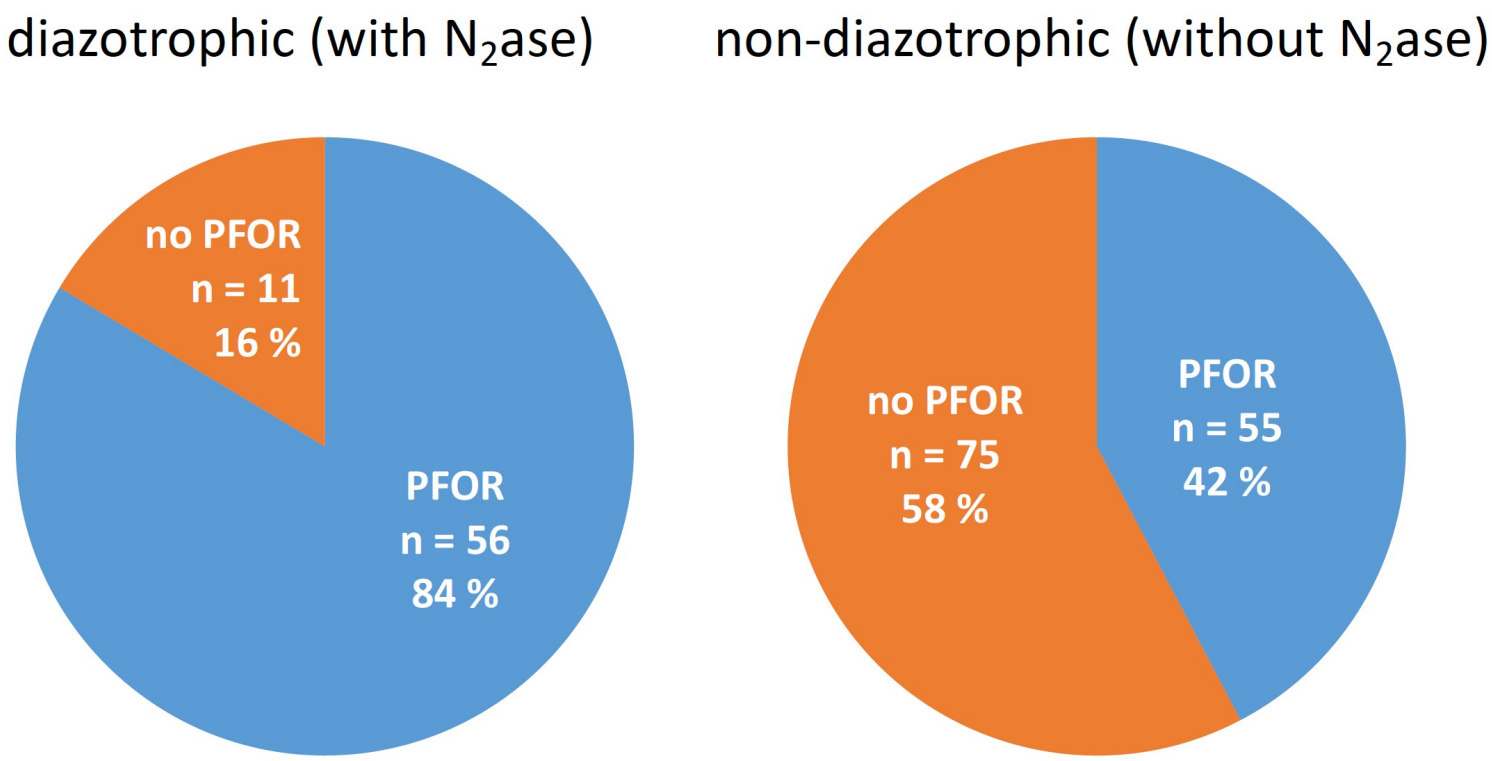

Figure 1- figure supplement 2

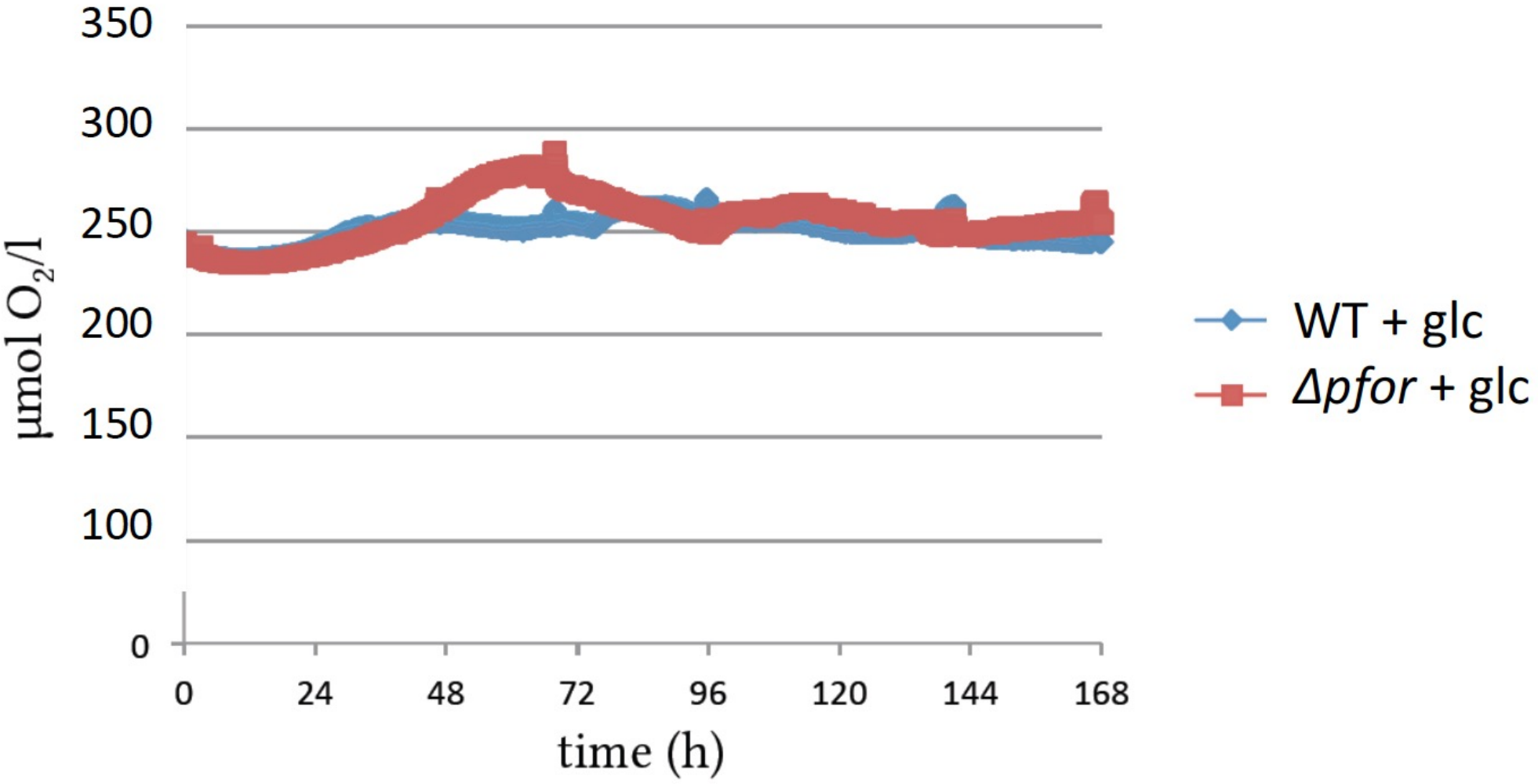

Figure 1- figure supplement 3

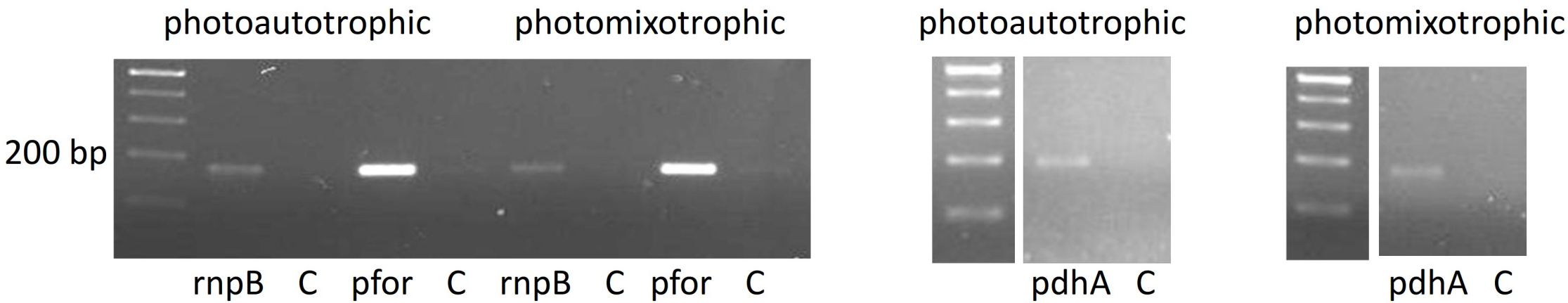

Figure 1- figure supplement 4

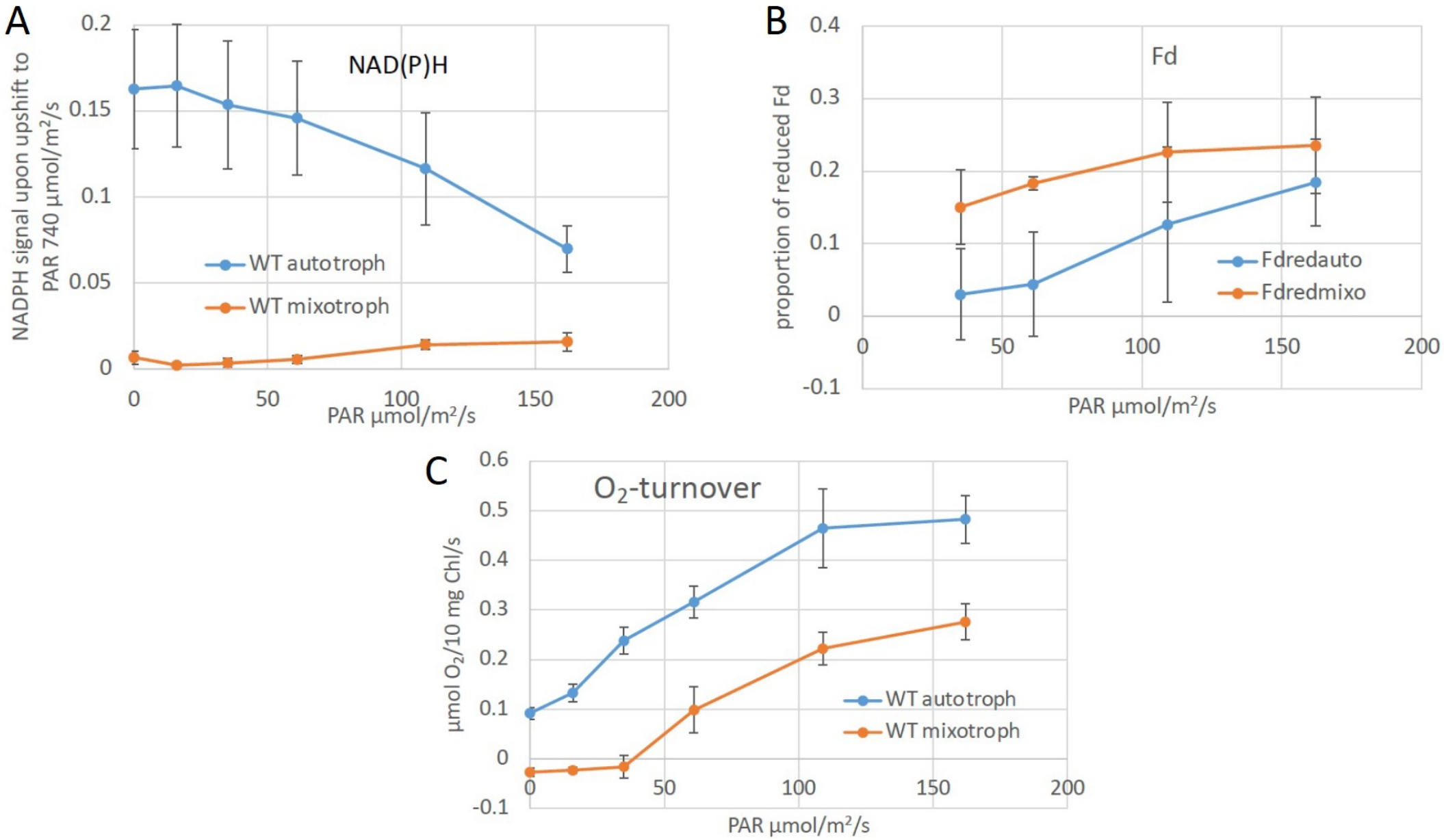

Figure 2

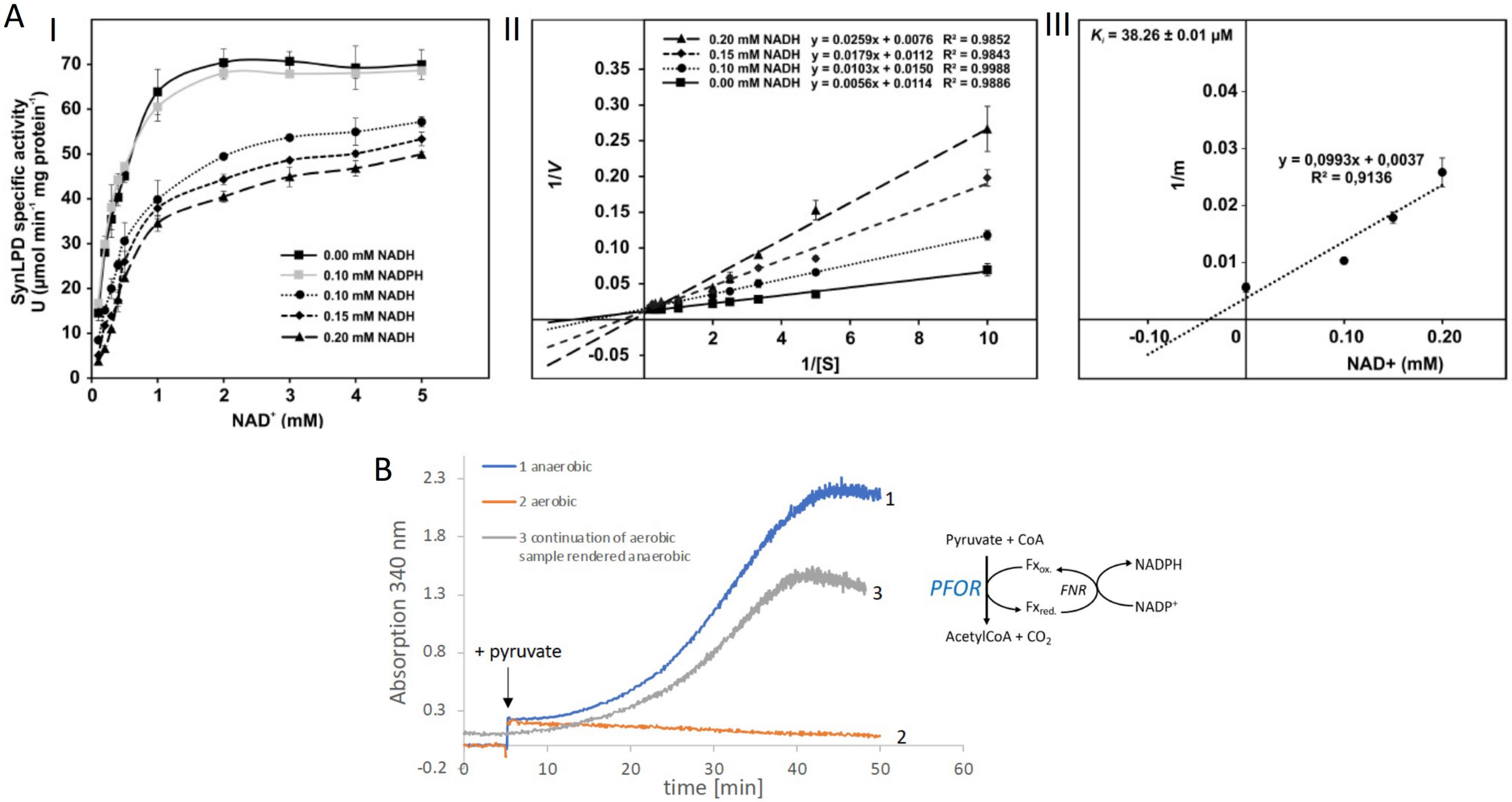
A
I
SynLPD specific activity
U (µmol min⁻¹ mg protein⁻¹)
NAD⁺ (mM)
0.00 mM NADH
0.10 mM NADPH
0.10 mM NADH
0.15 mM NADH
0.20 mM NADH
II
0.20 mM NADH y = 0.0259x + 0.0076 R² = 0.9852
0.15 mM NADH y = 0.0179x + 0.0112 R² = 0.9843
0.10 mM NADH y = 0.0103x + 0.0150 R² = 0.9988
0.00 mM NADH y = 0.0056x + 0.0114 R² = 0.9886
1/V
1/[S]
III
Ki = 38.26 ± 0.01 µM
y = 0,0993x + 0,0037
R² = 0,9136
1/m
NAD+ (mM)
B
1 anaerobic
2 aerobic
3 continuation of aerobic sample rendered anaerobic
Absorption 340 nm
+ pyruvate
time [min]
Pyruvate + CoA
PFOR
Fxox.
Fxred.
FNR
NADPH
NADP+
AcetylCoA + CO2

Figure 2- figure supplement 1

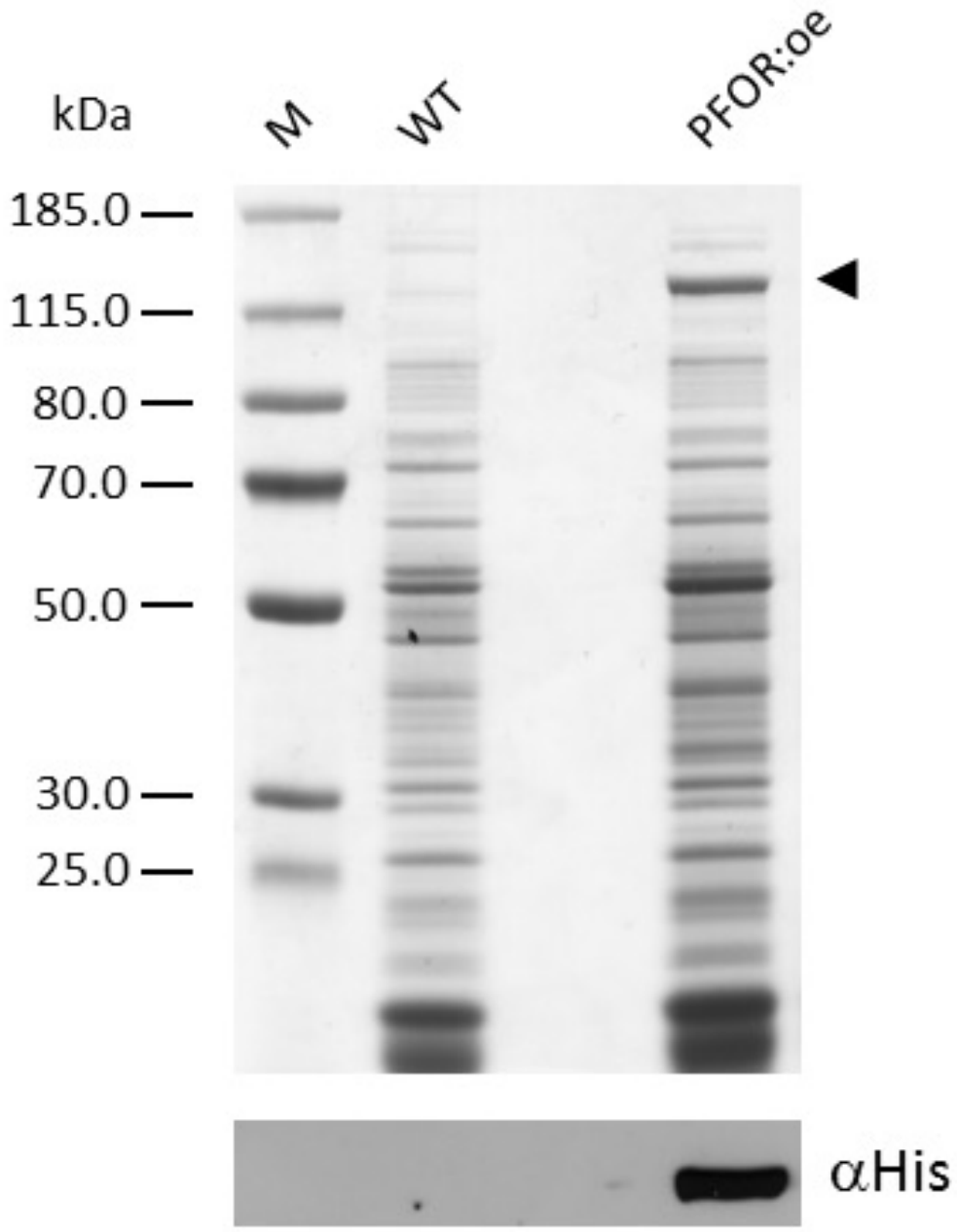

Figure 2- figure supplement 2

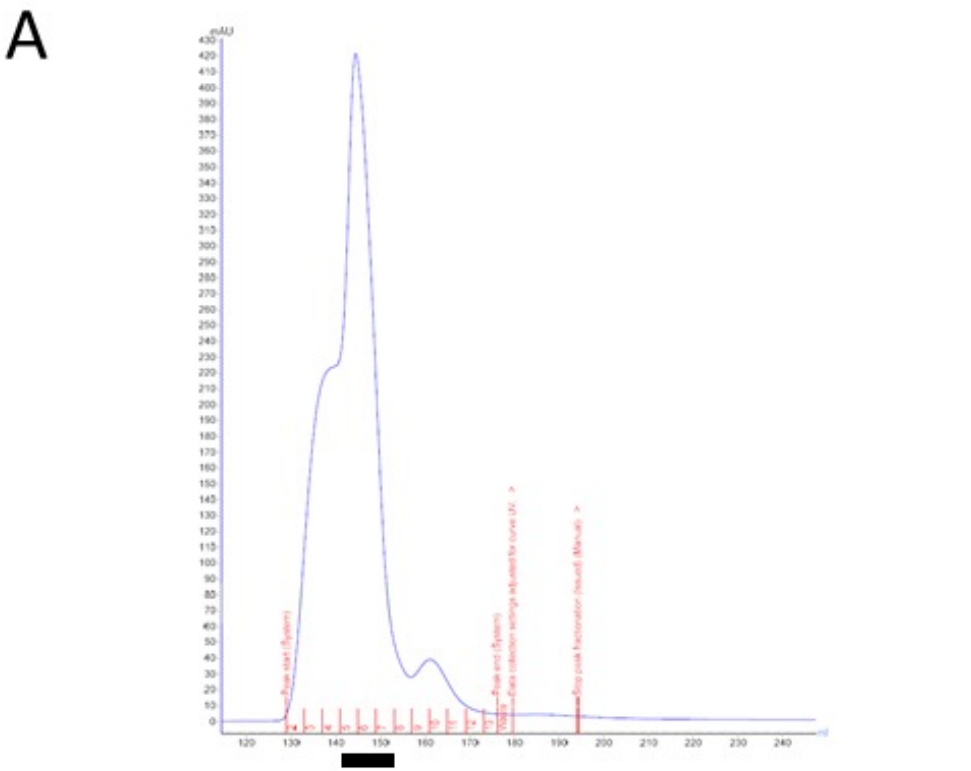

Figure 3

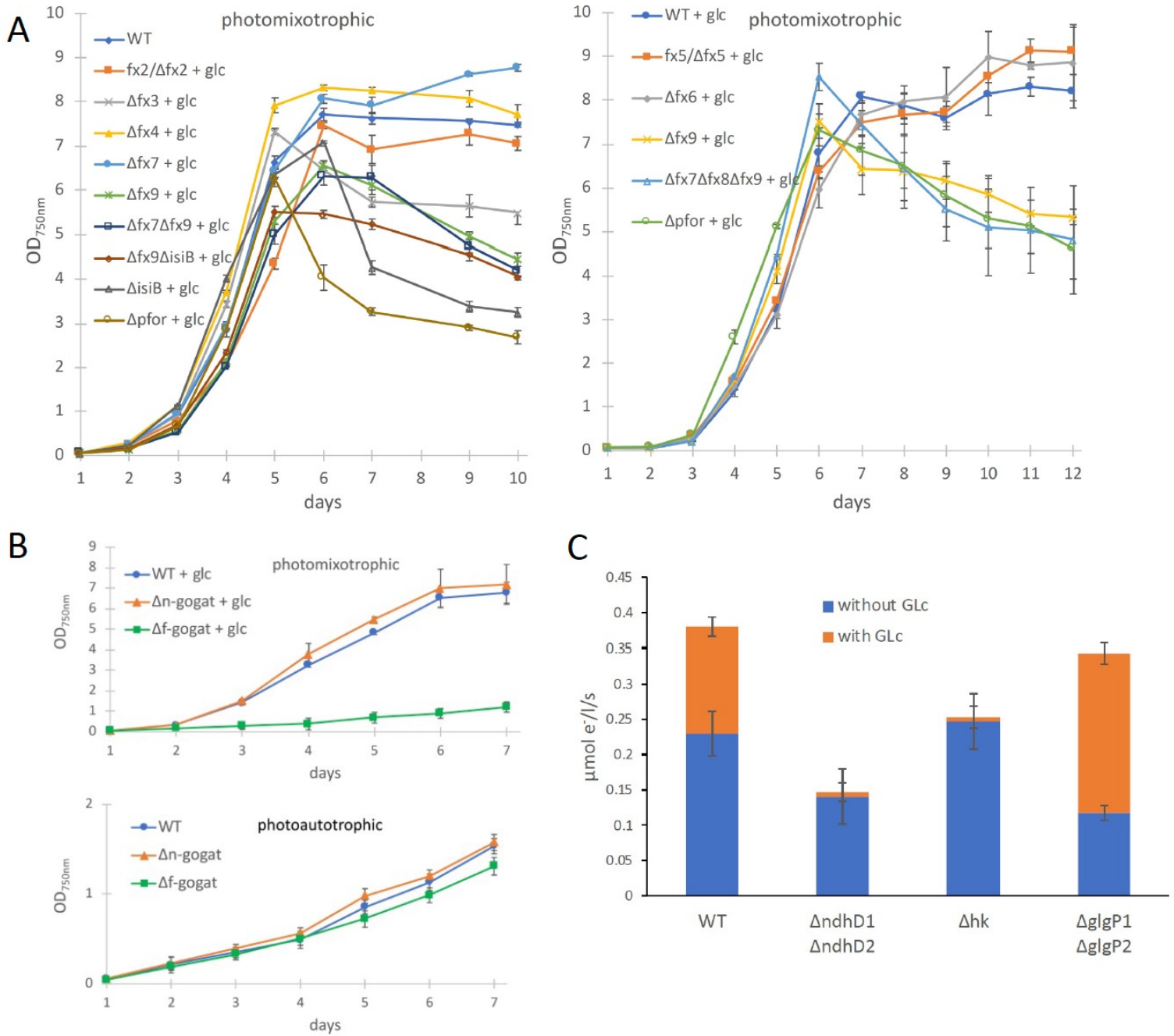
A
photomixotrophic
WT
fx2/Δfx2 + glc
Δfx3 + glc
Δfx4 + glc
Δfx7 + glc
Δfx9 + glc
Δfx7Δfx9 + glc
Δfx9ΔisiB + glc
ΔisiB + glc
Δpfor + glc
OD750nm
days
WT + glc
fx5/Δfx5 + glc
Δfx6 + glc
Δfx9 + glc
Δfx7Δfx8Δfx9 + glc
Δpfor + glc
B
photomixotrophic
WT + glc
Δn-gogat + glc
Δf-gogat + glc
photoautotrophic
WT
Δn-gogat
Δf-gogat
C
without GLc
with GLc
µmol e⁻/l/s
WT
ΔndhD1
ΔndhD2
Δhk
ΔglgP1
ΔglgP2

Figure 3 - figure supplement 1

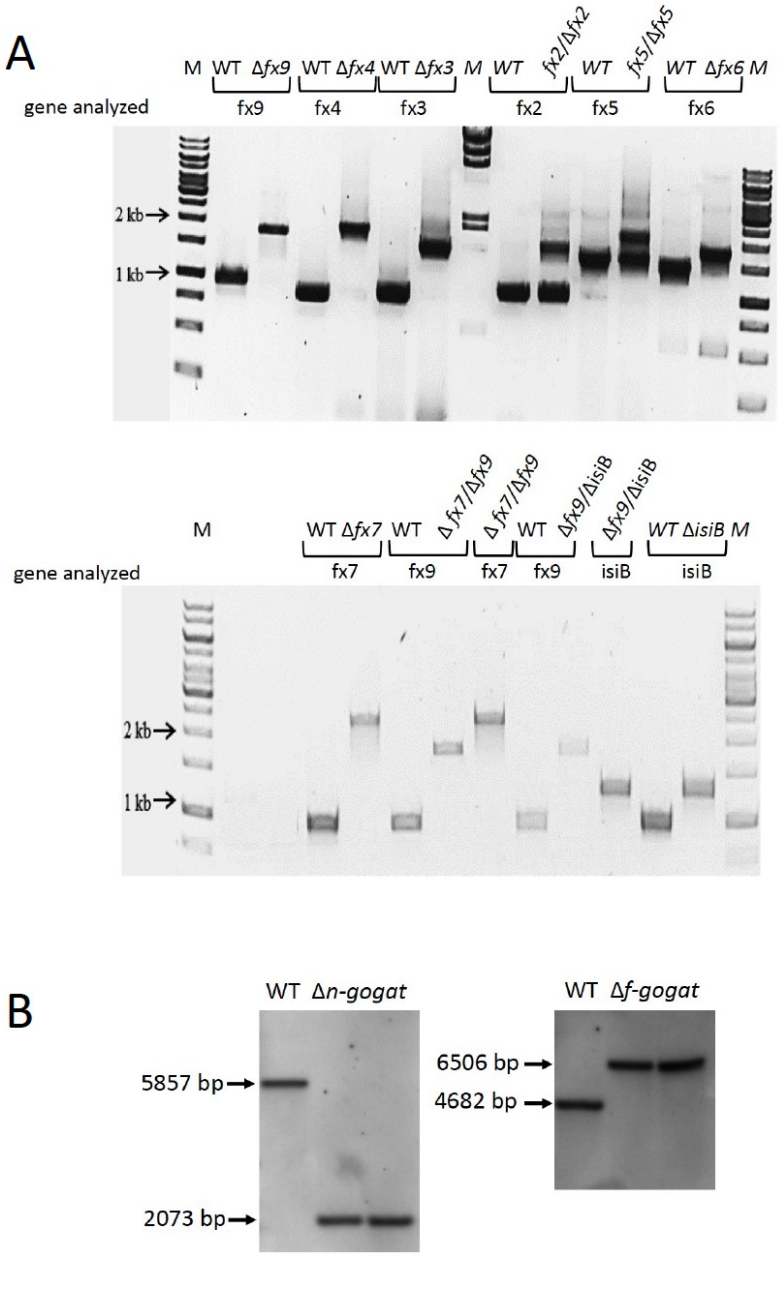

Figure 3- figure supplement 2

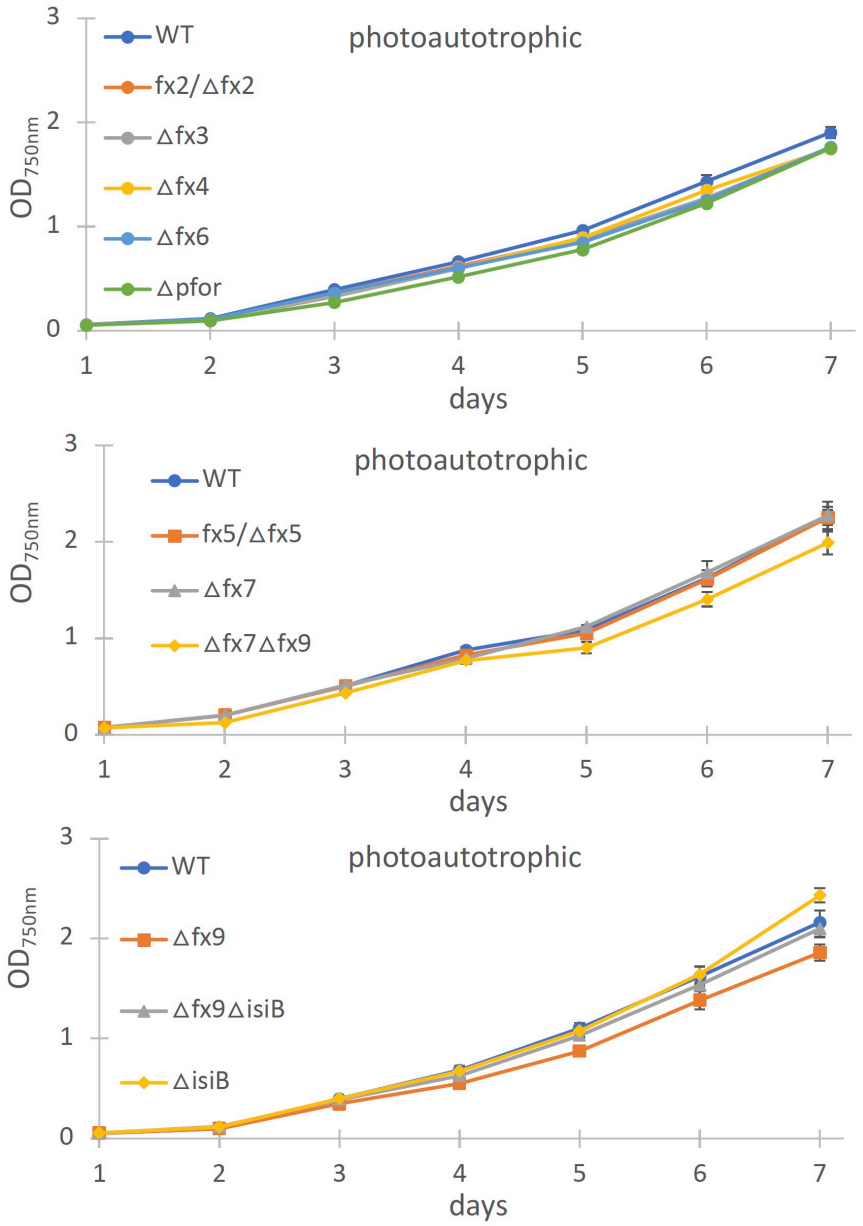

Figure 4

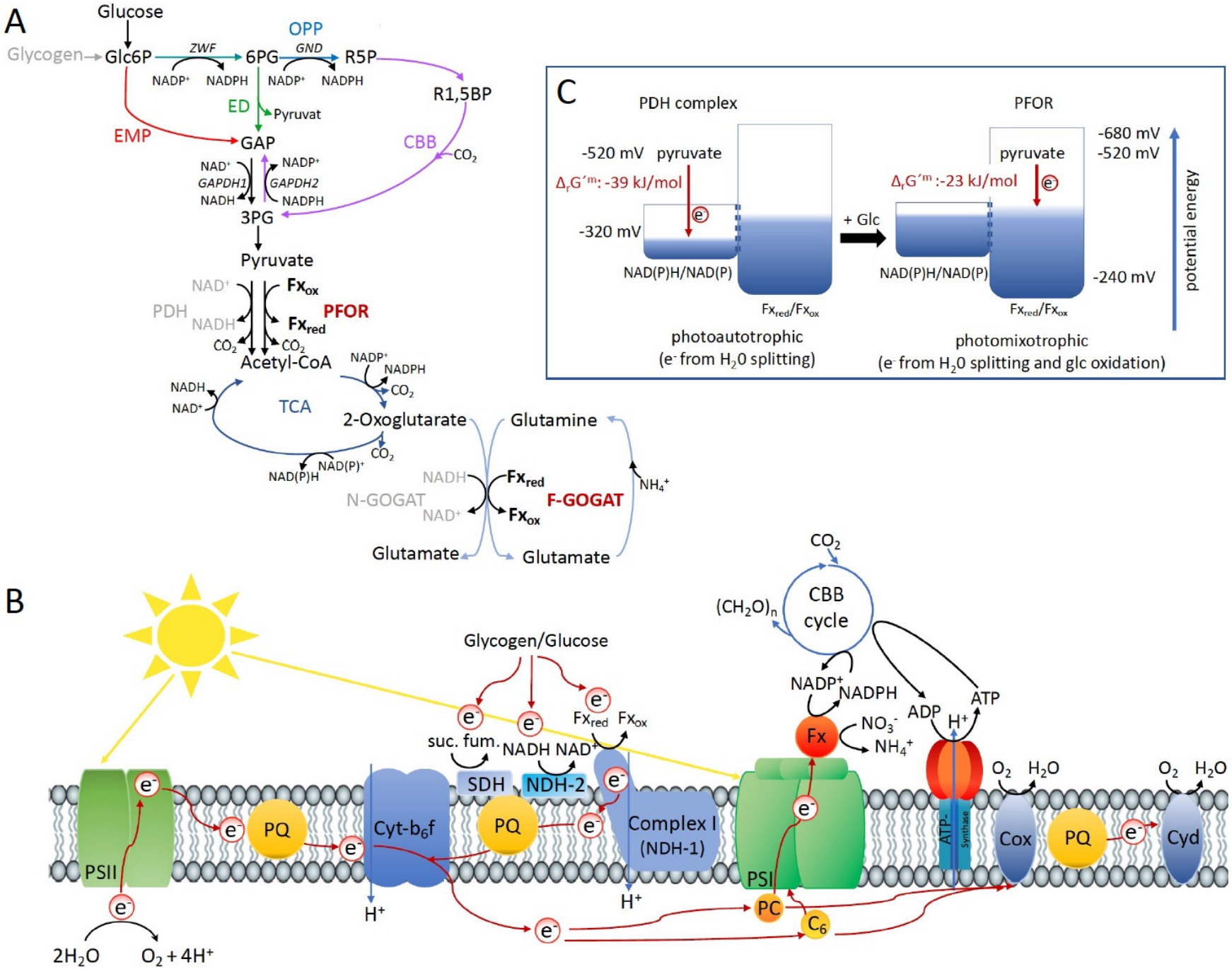
A
Glucose
Glycogen
Glc6P
ZWF
6PG
OPP
GND
R5P
NADP+
NADPH
R1,5BP
ED
Pyruvat
EMP
GAP
CBB
CO2
GAPDH1
GAPDH2
3PG
Pyruvate
PDH
PFOR
Fxox
Fxred
Acetyl-CoA
TCA
2-Oxoglutarate
Glutamine
Glutamate
N-GOGAT
F-GOGAT
NH4+
NAD(P)H
NAD(P)+
C
PDH complex
PFOR
-520 mV
pyruvate
ΔrG´m: -39 kJ/mol
-320 mV
NAD(P)H/NAD(P)
Fxred/Fxox
+ Glc
ΔrG´m :-23 kJ/mol
-680 mV
-520 mV
-240 mV
potential energy
photoautotrophic
(e- from H20 splitting)
photomixotrophic
(e- from H20 splitting and glc oxidation)
B
Glycogen/Glucose
(CH2O)n
CBB cycle
ATP
ADP
H+
Fx
NO3-
NH4+
suc. fum.
NADH NAD+
SDH
NDH-2
PQ
Cyt-b6f
Complex I (NDH-1)
PSII
PSI
PC
C6
Cox
Cyd
ATP-Synthase
2H2O
O2 + 4H+
O2
H2O